3-2020

Global Gradient-Based Phase Unwrapping Algorithm for Increased Performance in Wavefront Sensing

Bryan R. Bartelt

GLOBAL GRADIENT-BASED PHASE UNWRAPPING ALGORITHM FOR INCREASED PERFORMANCE IN WAVEFRONT SENSING

THESIS

Bryan R. Bartelt, Captain, USAF

AFIT-ENG-MS-20-M-006

DEPARTMENT OF THE AIR FORCE
AIR UNIVERSITY

AIR FORCE INSTITUTE OF TECHNOLOGY

Wright-Patterson Air Force Base, Ohio

AFIT-ENG-MS-20-M-006

GLOBAL GRADIENT-BASED PHASE UNWRAPPING ALGORITHM FOR INCREASED PERFORMANCE IN WAVEFRONT SENSING

THESIS

Presented to the Faculty

Department of Electrical and Computer Engineering

Graduate School of Engineering and Management

Air Force Institute of Technology

Air University

Air Education and Training Command

In Partial Fulfillment of the Requirements for the

Degree of Master of Science in Electrical Engineering

Bryan R. Bartelt, B.S.E.E.

Captain, USAF

26 March 2020

AFIT-ENG-MS-20-M-006

GLOBAL GRADIENT-BASED PHASE UNWRAPPING ALGORITHM FOR INCREASED PERFORMANCE IN WAVEFRONT SENSING

THESIS

Bryan R. Bartelt, B.S.E.E.
Captain, USAF

Committee Membership:

Stephen C. Cain, PhD
Chair

Maj David Becker, PhD
Member

Capt Joseph Tompkins, MS
Member

Abstract

As the reliance on satellite data for military and commercial use increases, more effort must be exerted to protect our space-based assets. In order to help increase our space domain awareness (SDA), new approaches to ground-based space surveillance via wavefront sensing must be adopted. Improving phase-unwrapping algorithms in order to assist in phase retrieval methods is one way of increasing the performance in current adaptive optics (AO) systems.

This thesis proposes a new phase-unwrapping algorithm that uses a global, gradient-based technique to more rapidly identify and correct for areas of phase wrapping during particular phase retrieval methods. This is beneficial in regard to the speed and accuracy within which a wrapped phase estimate is unwrapped using a new algorithm, and doing so without having to change current AO systems or physical setups.

Acknowledgements

I'd like to thank Dr. Cain, for his never-ending guidance and patience throughout my research and writing process. His expertise and dedication truly made my time at AFIT extremely fascinating, informative and enjoyable.

I'd also like to thank my wife, for her continued support and her never-wavering enthusiasm during my long nights and weekends of writing.

- Bryan Bartelt

Table of Contents

List of Figures

Page

List of Tables

Page

GLOBAL GRADIENT-BASED PHASE UNWRAPPING ALGORITHM FOR INCREASED PERFORMANCE IN WAVEFRONT SENSING

I. Introduction

On December 20, 2019, the United States Space Force was stood up in order to protect US and allied assets and ensure the peaceful use of space for all responsible actors, consistent with applicable law, including international law [1]. In order to achieve this mission, the ability to thoroughly survey all commercial, friendly and hostile space material is of utmost importance. Using ground-based imaging systems are among the most cost-effective and convenient ways to ensure the Space Force maintains its Space Domain Awareness (SDA). These imaging systems are vital to the detection and surveillance of known and unknown space objects in Geosynchronous, Low-Earth and Highly Elliptical orbits, as well as objects passing near to the earth.

There are three main areas of concern in space for the continued safeguarding of US assets and the Earth: space debris, micro-satellites and near-earth asteroids (NEAs) [2, 3, 4]. These all pose a threat to the earth and satellite networks that perform communication, security and research objectives for many public, private and state-run organizations, including the US Space Force and the US Department of Defense. In an already clustered

space environment where the number of all three of these threats are increasingly being detected, ground-based optical systems must continue to adapt new and improved image registration techniques that can account for the optical turbulence caused by the Earth's atmosphere.

1.1 Motivation

This thesis aims to explore a common ground-based image restoration method that compensates for phase aberrations due to atmospheric turbulence. This common method is to be implemented in wavefront sensors (WFS) in order to improve the quality of images collected. The theoretical method should work independently of an optical system's physical attributes, and solely seek to update and inform the system's WFS as quickly and accurately as possible.

These image restoration methods that attempt to counter atmospheric turbulence can be called phase retrieval. In mathematical terms, phase retrieval is described as recovering a complex signal, given only the magnitude-squared of its Fourier transform. This means that phase retrieval methods attempt to estimate the phase of a complex signal without any initial phase information given. This concept is used for many different signal and image processing problems.

However, unlike some other applications, when used in conjunction with telescope optics, information about the imaging system can also be included. This extra information includes the physical properties of the

imaging system and can help recover a better estimate of the unknown phase.

Phase retrieval methods used in telescopes and WFS's attempt to recover the unknown phase value from a wavefront that is incident to the system's aperture given only the intensity data, $I_d(x', y')$, in the detector plane. See Equations (1.1) & (1.2), where taking the Fourier Transform of $A(x, y)$, which is a mathematical 2-D representation of the aperture's shape and size, and $\theta(x, y)$, which is the unknown turbulent wavefront, results in the complex field in the detector plane, $H_d(x', y')$.

$$I_d(x', y') = |H_d(x', y')|^2 \tag{1.1}$$

$$H_d(x', y') = F\left\{A(x, y)e^{(-j\theta(x,y))}\right\} \tag{1.2}$$

In the effort to try and recover the unknown phase value, the estimated phase screens can become "wrapped" due to the limitations in both hardware and software. This is another hurdle that will be explored in this thesis.

1.2 Wavefront Sensors

Resolving an image of a space-based object from a ground-based imaging system can prove difficult when atmospheric turbulence is present. Wavefront sensors, which aim to counter the effects of atmospheric turbulence, sometimes need to operate around the millisecond level. This

ensures that the aberrations in the image can be measured and accounted for prior to the wavefront distorting the image further.

Common wavefront sensors, like the Shack-Hartmann WFS, consist of an array of small, identical lenses, called lenslets. When a plane wave is incident to the telescope pupil, these lenslets divide the light entering the aperture into sub-apertures that project the image onto a CCD at positions determined by the array's geometry. When the incident wave has been disrupted by the atmosphere, the images projected by the lenslets will no longer fall on the CCD in geometric fashion (See Figure 1). These displacement measurements are passed on to the other adaptive optics (AO) components and are used to account for the tilt aberrations caused by the atmosphere over each sub-aperture. Local tilt information can be used to reconstruct the wave front over the entire aperture.

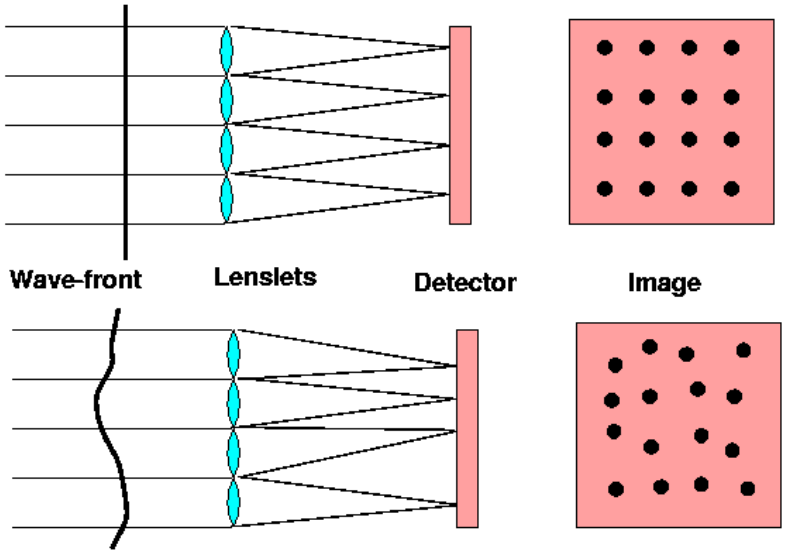

Figure 1: An example of how WFSs and lenslets detect atmospheric turbulence [5].

1.3 Thesis Overview

Exploring new phase unwrapping and phase retrieval methods will bolster the ability of ground-based telescopes to resolve and refine images taken through the atmosphere. This will increase the detection rates for space debris, micro-satellites and NEAs, resulting in more comprehensive SDA.

Chapter II lays the foundation with background information and assumptions needed to explore the concept of phase unwrapping and phase retrieval. Several existing phase retrieval methods, as well as related research are introduced to establish a baseline of knowledge for the reader. The new phase unwrapping approach is also examined.

Chapter III motivates the reader and outlines the materials and process used for simulation and comparison of the aforementioned phase unwrappers and phase retrieval methods. This chapter also analyzes the results from simulation, as the next chapter will examine the concepts with real world lab data.

Chapter IV dives into the feasibility of the phase unwrapping and phase retrieval methods by using collected lab data to evaluate and compared methods. The materials and process used for data collection and evaluation are discussed, as well as the results of the evaluation.

Chapter V concludes the thesis with a summary of takeaways from the comparisons of phase retrieval methods. Potential for future work is also discussed.

II. Background

As mentioned in Chapter 1, the method of phase retrieval is an extremely complex concept that has yet to be fully mastered or implemented to its fullest potential. This chapter covers the basic optical theory behind the phase retrieval problem and explores a few of the current methods that are used in detail.

2.1) Essential Optics Theory

This thesis builds upon many fundamentals of Fourier optics derived by Joseph Goodman [6]. Relevant subject matter includes the understanding of light propagation through wave-optics.

2.1.1) Light Propagation

It is well known that the propagation of light to a given location can be mathematically described using 2-D Fourier Transforms. In this thesis it is assumed that the light source being imaged by the ground-based telescope is normalized and far enough away to be considered a point source, with its phase, $\omega(x, y)$, described as a plane wave. These assumptions also satisfy the Fraunhofer propagation criteria [6]. Once the wavefront comes into contact with the Earth's atmosphere, it inherits an unknown phase delay, $\theta(x, y)$, which distorts the light incident to the telescope's aperture, $A(x, y)$. The phase delay is caused due to the "boiling effect" or churning and fluctuation in the density of the atmosphere [7]. Assuming the telescope is properly

focused on this normalized light source, and that $\omega(x,y)$ is a plane wave, the pupil function, $P(x,y)$, at the aperture of the telescope can be expressed as:

$$P(x,y) = e^{-j(\omega(x,y)+\theta(x,y))} \tag{2.1}$$

$$P(x,y) = A(x,y)e^{-j\theta(x,y)} \tag{2.2}$$

Propagating from the pupil plane to the telescope's detector plane can be mathematically expressed using a Fourier Transform, where (x,y) are coordinates in the pupil plane and (x',y') are coordinates in detector plane. Taking the magnitude squared of this propagation gives us the measured intensity, $I_d(x',y')$, on the detector plane.

$$I_d(x',y') = |F\{P(x,y)\}|^2 \tag{2.3}$$

This intensity pattern is the measured data that is of most interest to observers but is often distorted due to the phase delay, $\theta(x,y)$, caused by the atmosphere. Throughout this paper, the Lens Maker's equation is considered satisfied, which implies that there are no additional focus aberrations inherent to the intensity measurement.

2.1.2) Wave Front Construction

Expressing light's phase using Zernike polynomials is a common way to quantify the turbulence that the wave fronts acquire while traveling through the atmosphere. They are an orthogonal set of polynomials used to parameterize specific phase aberrations and carry coefficients to weight each

respective type of aberration. Figure 2 shows the aberration types that Zernike polynomials describe like piston, tilt, focus, astigmatism, coma, and more.

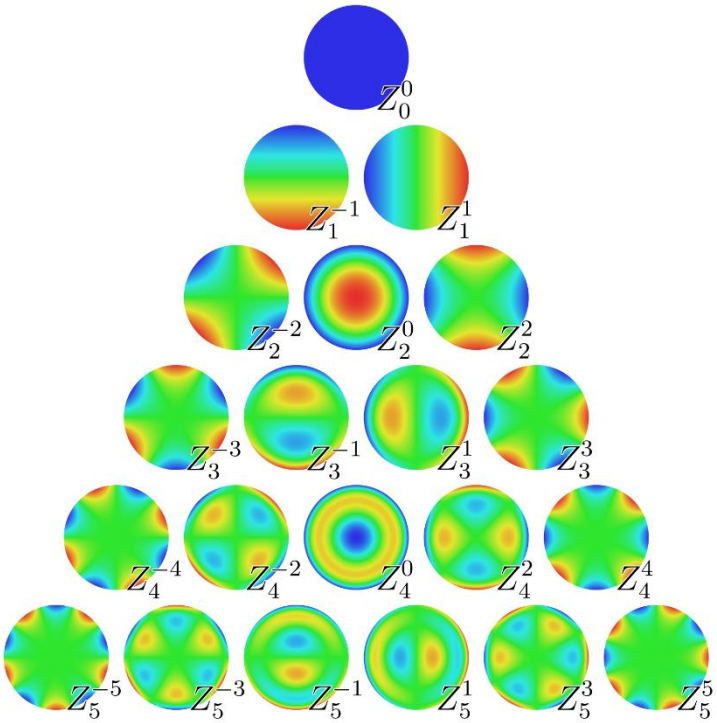

Figure 2: Phase descriptions of the first 21 Zernike polynomials [8].

Due to their orthogonality, these polynomials, $\phi_n(x, y)$, and their respective coefficients, z_n, can be summed together to create a simulated phase screen, $\theta(x, y)$. See Equation (2.4) below.

$$\theta(x, y) = \sum_{n=1}^{N} z_n \phi_n(x, y) \tag{2.4}$$

All of the phase screens in this thesis do not include piston error, or z_1, as this is a term for delay and does not affect the shape of the wavefront.

As shown above, it is easy to see how a wavefront can be constructed using Zernike coefficients, but in some instances, it is important to know how to derive Zernike coefficients given only a wavefront, $\theta(x, y)$. This is done using a decomposition of the wavefront into coefficients as shown below.

$$z_n = \frac{\sum_x \sum_y \theta(x, y)\phi_n(x, y)}{\sum_x \sum_y \phi^2{}_n(x, y)} \tag{2.5}$$

The comprehension of both Zernike polynomials and basic light propagation are crucial in the understanding of imaging systems, wavefront sensors, and the motivation behind phase retrieval.

2.2) Phase Retrieval

As stated in Section 1.1, phase retrieval is the attempt to reconstruct the complex wavefront of a light source given only the measurement of its intensity. It is a technique used in ground-based imaging systems that drive optical components to account for atmospheric turbulence, helping to create a more resolute image in the detector plane. Mathematically, phase retrieval can be expressed as in Equation (2.6). Where $\theta(x, y)$ is the phase attempting to be recovered given $I_d(x', y')$.

$$I_d(x', y') = |F\{A(x, y)e^{-j\theta(x,y)}\}|^2 \tag{2.6}$$

The following phase retrieval methods seek to reconstruct $\theta(x, y)$ using iterative or gradient based approaches with a focus in Zernike polynomials.

2.2.1) The Intensity Based Least Squares Method

This phase retrieval method is a gradient decent method that seeks to determine the value of Zernike coefficients that best model the true phase using an iterative sum of squared errors comparison of the measured PSF and estimated PSF [9]. The process begins by choosing a step size, Δ, and a guess phase, $\theta_i(x,y)$, built from a set of N Zernike coefficients. Next, new estimation wavefronts are created by altering each Zernike coefficient, one at a time by +Δ and -Δ. This results in $2N$ new wavefronts, each one differencing positively and negatively by Δ. We will call this process of altering Zernike coefficients by Δ, 'stepping,' and W will represent an array of the newly constructed wavefronts.

$$W = \begin{pmatrix} \theta_{2+} = \theta_i + \Delta\phi_2(x,y) \\ \theta_{2-} = \theta_i - \Delta\phi_2(x,y) \\ \theta_{3+} = \theta_i + \Delta\phi_3(x,y) \\ \theta_{3-} = \theta_i - \Delta\phi_3(x,y) \\ \vdots \\ \theta_{N+} = \theta_i + \Delta\phi_N(x,y) \\ \theta_{N-} = \theta_i - \Delta\phi_N(x,y) \end{pmatrix} \tag{2.7}$$

Once the new wavefronts are produced, their intensity's can be computed using Equation (2.6). The $2N$ newly estimated intensity models can then be compared to the true measured PSF. The resulting comparison that yields the minimum sum of squared error passes on their respective Zernike coefficients that become the new guessed wavefront, $\theta_i(x,y)$, for the next iteration of the Intensity Based Least Squares (IBLS) method. Below, the

comparisons between the PSFs are calculated where $\hat{I}_d(x', y')$ is the true, measured PSF, and $I_W(x', y')$ is each estimated PSF and Q_w is the sum squared error associated between the two.

$$Q_W = \sum_x \sum_y [\hat{I}_d(x', y') - I_W(x', y')]^2 \tag{2.8}$$

This iterative process is continued until a maximum amount of iterations has been met, or Q_w breaks an error threshold, producing an estimate of the true waveform through Zernike coefficients. It is worth mentioning that this method performs better if something is already known about the incident phase screen and its respective Zernike coefficients prior to the first iteration.

2.2.2) The Electric Field Correlation Method

There is another phase retrieval method that uses Zernike coefficient stepping and estimation but instead uses the estimate electric-field in the detector plane. Similar to the IBLS, the Electric-Field Correlation (EFC) method evaluates a model of the system's E-field, and a set of altered, Zernike-weighted E-fields. The initial E-field model, $\hat{H}(x', y')$, is calculated by propagating a given, user-chosen, input phase derived from Zernike coefficients, $\theta_i(x, y)$, through the known aperture of the optical system.

$$\hat{H}(x', y') = F\{A(x, y)e^{-j\theta_i(x,y)}\} \tag{2.9}$$

Similar to the IBLS algorithm, this technique produces estimation wavefronts by altering N Zernike coefficients by a pre-determined step size, Δ. Next a comparison of the $2N$ estimated electric fields, $H_w(x', y')$, versus the modeled electric field, $\hat{H}(x', y')$ is calculated by seeing how correlated they are.

$$\rho_W(\hat{H}(x',y'),H_W(x',y')) = \frac{\sum_x \sum_y \hat{H}(x',y'),H_W(x',y')^*}{\sqrt{\sum_x \sum_y \hat{H}(x',y')\hat{H}(x',y')^*} \cdot \sqrt{\sum_x \sum_y H_W(x',y')H_W(x',y')^*}}$$

(2.10)

The estimated electric field with the highest correlation value, ρ_W, will have its respective Zernike coefficients used to build the input wavefront for the next iteration. Like the IBLS method, this iterative process is continued until a maximum amount of iterations has been met, or ρ_W breaks a threshold, producing an estimate of the true Zernike coefficients and inherently an estimate of the true waveform. It is worth mentioning that this method performs better if something is already known about the incident phase screen and its respective Zernike coefficients prior to the first iteration.

2.2.3) The Gerchberg-Saxton Method

Another common phase retrieval method was conceived by R.W. Gerchberg and W.O. Saxton in the 1980's [10]. This iterative method begins

with the known intensity measurement, the aperture's physical characteristics and a guess at the wavefront adherent to the aperture.

Gerchberg and Saxton used simple Fourier optics to propagate and reverse-propagate the wavefront back and forth from the detector plane to the aperture plane ensuring that the true aperture, $A(x,y)$, and measured intensity, $\hat{I}_d$, are inputted before each propagation, while the phase value is left to fluctuate. This can be shown in the 4 steps below.

$$\begin{aligned} &F^{-1}\{\sqrt{\hat{I}_d(x',y')}e^{-j\theta(x',y')}\} = A'(x,y)e^{-j\phi(x,y)} \\ &A'(x,y)e^{-j\phi(x,y)} \rightarrow A(x,y)e^{-j\phi(x,y)} \\ &\left|F\{A(x,y)e^{-j\phi(x,y)}\}\right| = \sqrt{I_d(x',y')}e^{-j\theta(x',y')} \\ &\sqrt{I_d(x',y')}e^{-j\theta(x',y')} \rightarrow \sqrt{\hat{I}_d(x',y')}e^{-j\theta(x',y')} \end{aligned} \tag{2.11}$$

This method can eventually lead to the phase converging closely to what the original incident phase screen looked like if the first guessed phase was chosen wisely. A parabolic wavefront of any type is usually a good choice for the guess input phase.

An issue with this method is that it outputs a wrapped phase. Phases are wrapped when the phase exceeds values of -π or π radians, which results in the algorithm losing track of how many radians the phase has spanned. This can happen with turbulent wavefronts and the more iterations of Gerchberg-Saxton that are executed, the more wrapped the phase becomes.

2.2.4) Phase unwrapping

As discussed, the Gerchberg-Saxton phase retrieval method concludes with a wrapped phase, where all values are constrained between -π and π radians. This is a common problem among other optical devices and algorithms, where the surpassing of 360 degrees cannot be accounted for due to excess noise, discontinuities or software limitations. Currently one of the industry standards for phase unwrapping, and one of the techniques that will be explored further in this paper, is the Calibrated Phase Unwrapping based on Least-Squares and Iterations (CPULSI) [11]. Although it excels with generic noisy wrapped phases, its performance seems to depreciate when there are moments of discontinuity across the wavefronts from places like a telescope aperture. See Figure 3 below. This technique will be referred to in this paper as the Least Squares Unwrapper (LSU).

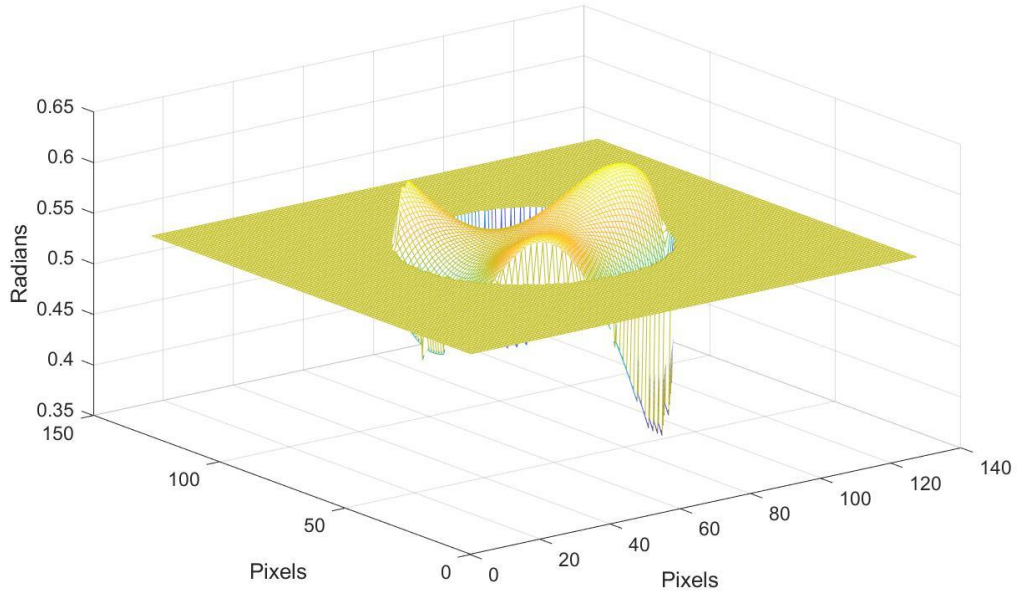

Figure 3: An example of a generated phase screen with discontinuity caused by an aperture.

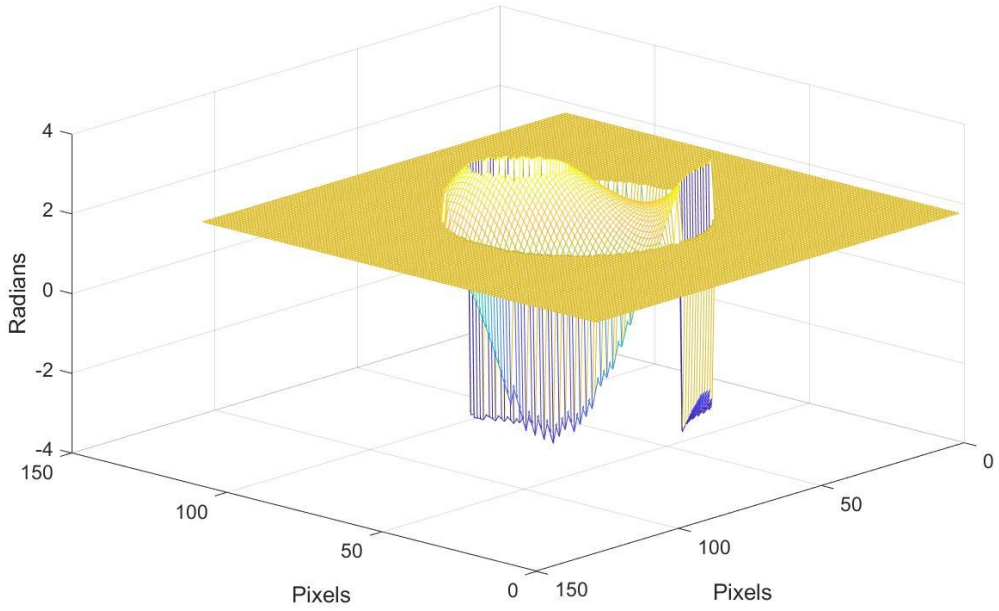

Figure 4: An example of a generated wrapped phase screen.

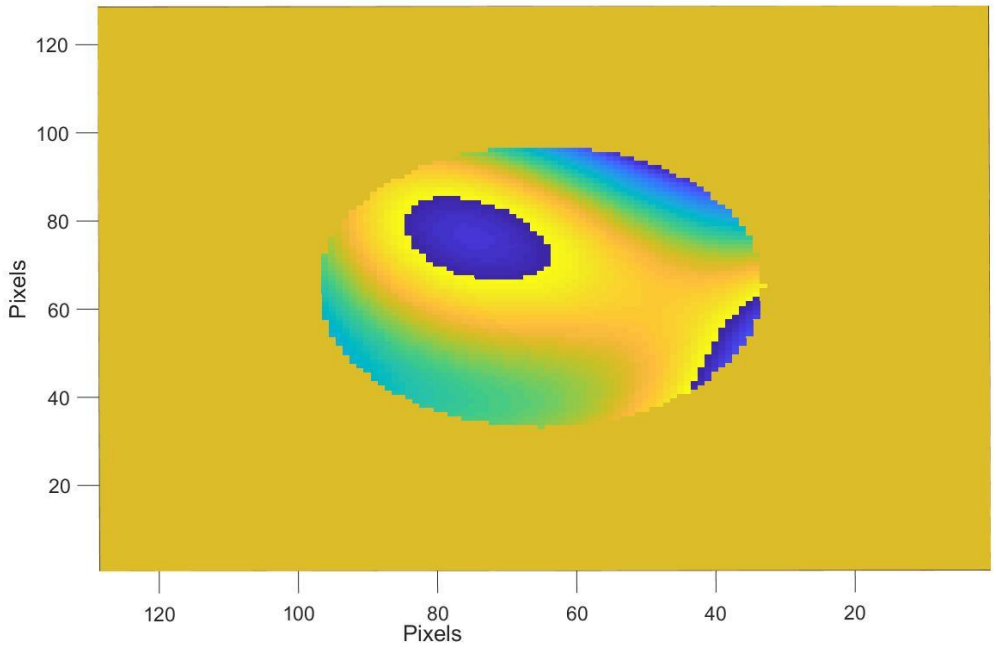

Figure 5: An overhead look at the wrapped phase screen from Figure 4.

The proposed phase unwrapping technique attempts to unwrap phase screens with large amounts of noise, as well as more effectively account for moments of discontinuity. This iterative, gradient-based approach will theoretically unwrap phase screens more quickly and more accurately given optical systems that have places of discontinuity. This method will be referred to as the Gradient-Based Unwrapper (GBU). To begin, it can be helpful to think about a wrapped phase as in Equation (2.12) below, where $K(x, y)$ is a matrix consisting of negative and non-negative integer values, $\theta(x, y)$ is a turbulent phase screen, and $\tilde{\theta}(x, y)$ is its wrapped phase.

$$\theta(x, y) = \tilde{\theta}(x, y) + 2\pi K(x, y) \tag{2.12}$$

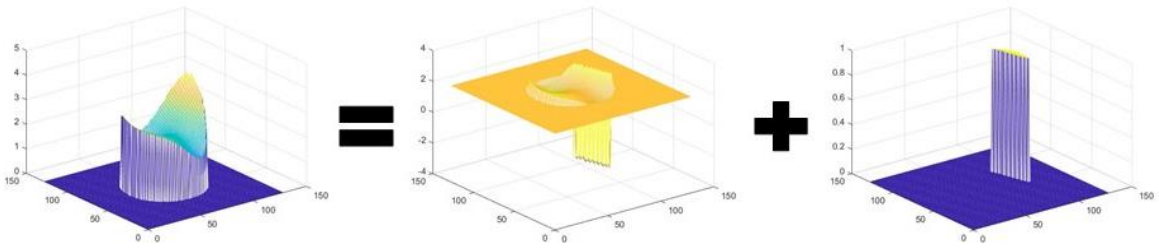

Figure 6: Wrapped phases are true phases that have exceeded a threshold of +/- 2π radians.

The $K(x, y)$ matrix attempts to locate the moments where the phase is wrapped, and to add or subtract the lost amounts of 2π radians of delay across phase screen. Note: in the first iteration of the GBU, the $K(x, y)$ matrix is initially set to zero.

The first computation involves the GBU attempting to solve for the Zernike coefficients, z_n, of the inputted wrapped phase, $\tilde{\theta}(x,y)$, using Equation (2.5).

$$z_n = \frac{\sum_x \sum_y \tilde{\theta}(x,y)\phi_n(x,y)}{\sum_x \sum_y \phi^2{}_n(x,y)} \tag{2.13}$$

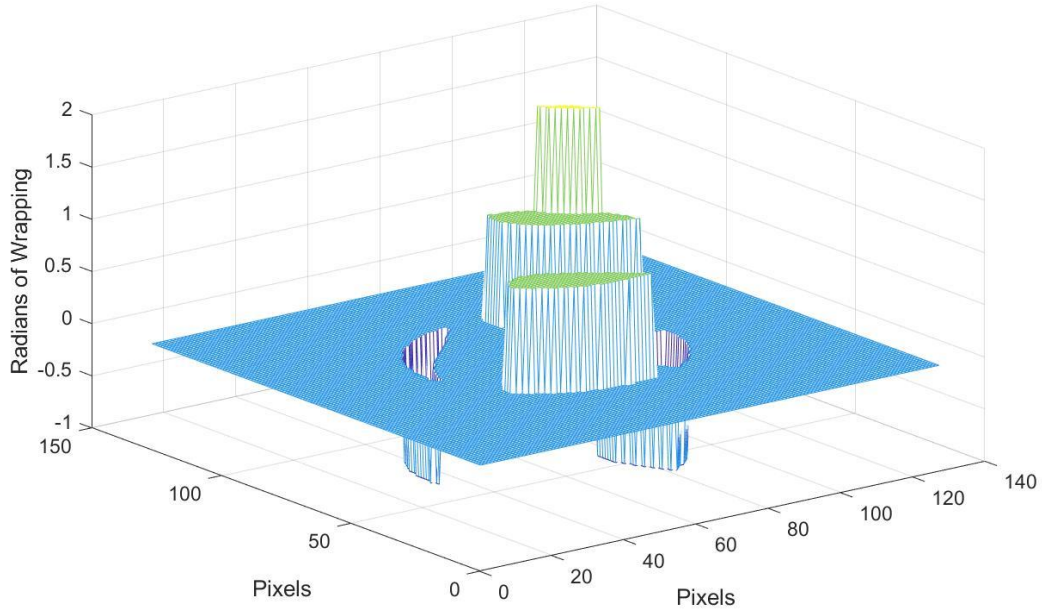

Figure 7: An example of the K(x,y) matrix, which attempts to locate the regions where the phase wraps and seeks to add radians back to the wrapped phase with integer values.

Using these estimated Zernike coefficients, a new phase screen is constructed $\theta_i(x,y)$, as the first iteration's guess at the true phase.

Next the GBU calculates the sum squared error between $\theta_i(x,y)$ and $\tilde{\theta}(x,y)+2\pi K(x,y)$. This error value Q_i, is stored for the next iteration.

$$Q_i = \sum_x \sum_y \left(\theta_i(x,y) - \tilde{\theta}(x,y) - 2\pi K(x,y) \right)^2 \tag{2.14}$$

Next, the gradient of the difference between $\theta_i(x,y)$ and $\tilde{\theta}(x,y)$ in respect to $K(x,y)$ is evaluated to identify the moments of wrapping.

$$\frac{dQ}{dK(x_0,y_0)} = -4\pi \sum_x \sum_y \left(\left(\theta(x_0,y_0) - \tilde{\theta}(x,y) - 2\pi K(x,y) \right) \frac{dK(x,y)}{dK(x_0,y_0)} \right)$$

(2.15)

$$\frac{dQ}{dK(x_0,y_0)} = -4\pi \left(\theta(x_0,y_0) - \tilde{\theta}(x,y) - 2\pi K(x_0,y_0) \right) \tag{2.16}$$

The moments where the gradient exceeds the threshold correspond to the regions where $K(x,y)$ will be increased or decreased by one.

$$K(x,y) = \begin{bmatrix} \text{if } \dfrac{dQ_i}{dK(x_0,y_0)} < -\pi & K(x_0,y_0) = -1 \\ \text{if } \dfrac{dQ_i}{dK(x_0,y_0)} > \pi & K(x_0,y_0) = 1 \\ \text{Otherwise} & K(x_0,y_0) = 0 \end{bmatrix} \tag{2.17}$$

Once $K(x,y)$ is revised with the logic above, the iteration is complete. $K(x,y)$ and $\theta_i(x,y)$ are then passed onto the next iteration. The algorithm is considered converged when the difference between the error values of consecutive iterations, Q_i and Q_{i-1} are lessened to beat a user defined threshold. This infers that the algorithm could not find any other regions to compensate for lost radians in the wrapped phase.

2.2.5) Zingarelli Combined Method

Unfortunately, gradient decent methods, like the IBLS, often get trapped in local minima [9]. Others, like Zingarelli, have attempted to avoid problems like this by combining techniques. Zingarelli's resulting method involves the IBLS and EFC algorithms, plus the Gerchberg-Saxton phase retrieval method.

Using the intensity measurement, Zingarelli first estimates the E-field through an iteration of the Gerchberg-Saxton method in order to retrieve estimated Zernike coefficients from the EFC method. Once the Zernike coefficients are estimated, they become the initial conditions for the IBLS method.

The output of the IBLS method produces Zernike coefficients as well that create a phase that is checked against a error threshold. If this threshold is not breached, then the phase is used as the input guess for another iteration of the GS algorithm, which initiates another iteration of the whole process.

This method has been shown to improve the accuracy for phase retrieval problems, but its speed and feasibility in wavefront sensors have not been tested.

III. MATLAB Simulation

In this chapter, MATLAB R2018a was used to test, evaluate and compare the different phase retrieval methods to the proposed method. The computer used to perform this simulation possessed an 8th generation, i7 core processor. For both situations the impulse responses of the telescope, or in an optical system's case: the Point Spread Functions (PSFs), were generated with known waveform aberrations. These aberrations are known to the observers but are not passed on to the phase retrieval methods as any sort of initial parameter and will have no effect on the performance of any of the methods.

Another condition of the simulation is that each PSF was measured independently in time to all other PSFs. Therefore, this simulation is theoretically built to evaluate completely independent short exposure frames of an optical system (>20ms). The wavelength of the light theoretically does not matter, meaning that the following techniques could be used in any imaging system for any region of the electromagnetic spectrum.

3.1) MATLAB Simulation Methodology

The MATLAB simulations rely upon creating PSFs using a mathematical representation of an optical system's physical features, as well as the using the generation of turbulent, statistically independent, wavefronts.

The particular scenario being looked at for the following simulations are that of an optical system undergoing an attempt to image a single star, given an arbitrary wavelength, from Earth's surface. The star in question is far enough away from Earth to be considered a perfect point source. The resulting PSFs, phase screens and optical system aperture are all expressed via 128x128 pixel matrices, with the circular pupil of the aperture having a diameter of 64 pixels. This leaves an area of discontinuity across the aperture like a true telescope as shown in Figure 7.

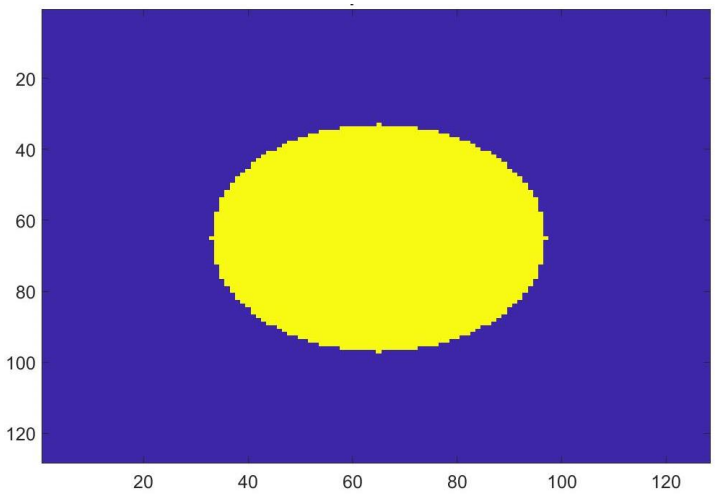

Figure 8: Simulated telescope aperture.

3.1.1) Generating Random Turbulent Phase Screens

First, the turbulent phase screen is calculated based on a finite set of Zernike polynomials with coefficients, z_n. This set of coefficients, $\vec{Z}$, will represent the random atmospheric aberrations to the simulated optical system: focus, astigmatism, coma, etc.

$$\vec{Z} = \begin{pmatrix} z_1 \\ z_2 \\ \vdots \\ z_n \end{pmatrix} \tag{3.1}$$

In order to build a realistic phase screen, we need to account for the Zernike Coefficient's covariance. According to Roddier [12], a spectral decomposition of the coefficients is required. This is achieved by using a Cholesky Factorization effort once the coefficient's covariance matrix is found.

Using Noll's derivation given that the Zernike coefficients are Gaussian random variables, with zero mean, the resulting covariance matrix, C, for the Zernike coefficients is given below [13].

$$C = \begin{bmatrix} 0.4536 & 0 & 0 & 0 & 0 & 0 & -0.0143 & 0 & 0 & 0 \\ 0 & 0.4536 & 0 & 0 & 0 & -0.0143 & 0 & 0 & 0 & 0 \\ 0 & 0 & 0.0235 & 0 & 0 & 0 & 0 & 0 & 0 & -0.0039 \\ 0 & 0 & 0 & 0.0235 & 0 & 0 & 0 & 0 & 0 & 0 \\ 0 & 0 & 0 & 0 & 0.0235 & 0 & 0 & 0 & 0 & 0 \\ 0 & -0.0143 & 0 & 0 & 0 & 0.0063 & 0 & 0 & 0 & 0 \\ -0.0143 & 0 & 0 & 0 & 0 & 0 & 0.0063 & 0 & 0 & 0 \\ 0 & 0 & 0 & 0 & 0 & 0 & 0 & 0.0063 & 0 & 0 \\ 0 & 0 & 0 & 0 & 0 & 0 & 0 & 0 & 0.0063 & 0 \\ 0 & 0 & -0.0039 & 0 & 0 & 0 & 0 & 0 & 0 & 0.0025 \end{bmatrix} \tag{3.2}$$

These values theoretically make sense because we know that the lower order Zernike polynomials carry more of the phase screen's error. Luckily, wave front sensors are able to automatically adjust for the tilt coefficients, z_2 and z_3. This is achieved by the sensor automatically tracking the PSF across

the detector plane using a center of mass technique. This infers that the tilt coefficients can be ignored, and the algorithms can focus solely on estimating the higher order Zernike's (z_4 and higher), and not have to worry about the position of the PSF.

Next, the overall magnitude of C also changes depending on the relationship between the diameter of the system's aperture, D, and the Fried parameter, $r0$, which is a scalar measurement of the quality of optical transmission through the atmosphere.

The ratio of $D/r0$ has a direct effect on the magnitude of turbulence seen in the generated waveform, and therefore a direct effect on the resulting noise seen in the PSF. In order to mitigate the effects of the atmosphere, most wave front sensors are designed with the average Fried parameter value of the surrounding environment in mind. This keeps the ratio of $D/r0$ as close to 1 as possible as often as possible. The resulting equation, based on coefficients z_4 through z_{11}, is computed to be:

$$C = \left(\frac{D}{r0}\right)^{(5/3)} \begin{bmatrix} 0.0235 & 0 & 0 & 0 & 0 & 0 & 0 & -0.0039 \\ 0 & 0.0235 & 0 & 0 & 0 & 0 & 0 & 0 \\ 0 & 0 & 0.0235 & 0 & 0 & 0 & 0 & 0 \\ 0 & 0 & 0 & 0.0063 & 0 & 0 & 0 & 0 \\ 0 & 0 & 0 & 0 & 0.0063 & 0 & 0 & 0 \\ 0 & 0 & 0 & 0 & 0 & 0.0063 & 0 & 0 \\ 0 & 0 & 0 & 0 & 0 & 0 & 0.0063 & 0 \\ -0.0039 & 0 & 0 & 0 & 0 & 0 & 0 & 0.0025 \end{bmatrix}$$

(3.3)

Then, the result of a Cholesky factorization of the covariance matrix, W, can be used to calculate a set of true Zernike coefficients, $\vec{\hat{Z}}$, using the following formula [12]. Where $\vec{n}$ is a set of Gaussian random variables with zero mean and unit variance.

$$C = WW^T \tag{3.4}$$

$$\vec{\hat{Z}} = \vec{n}W \tag{3.5}$$

Now we are able to accurately depict a distorted wavefront due to atmospheric optical aberrations. The resulting randomly generated phase screen, $\hat{\theta}(x,y)$, is computed using a sum of the products of the true aberration values, $\hat{z}_n$, and their respective Zernike polynomials, $\phi_n(x,y)$.

$$\hat{\theta}(x,y) = \sum_{n=4}^{11} \hat{z}_n \phi_n(x,y) \tag{3.6}$$

Note that the covariance values in C are subject to change if the Zernike coefficient's variances are altered.

3.1.2) Generating Point Spread Functions

Next, the physical characteristics of the optical system's aperture, $A(x,y)$, are considered and mathematically described (usually as a *rect* or *circ* function) and multiplied with the incident waveform's complex field as show below to produce the system's pupil function, $P(x,y)$.

$$P(x,y) = A(x,y)e^{-j\hat{\theta}(x,y)} \tag{3.7}$$

Finally, we can produce the simulated PSF, $\hat{I}_d(x', y')$, by taking the magnitude and square of the two-dimensional Fourier transform of the pupil function [6]. The PSF is the only bit of information known to the observer and is the only bit of measured data passed to the phase retrieval algorithms.

$$\hat{I}_d(x', y') = \left| F\left\{P(x, y)\right\}\right|^2 \tag{3.8}$$

An example of what a non-turbulent PSF, where $\hat{\theta}(x, y)$ is a plane wave, and therefore has Zernike coefficient values equal to 0, would look like is shown below in Figure 8. Assume $D/r0 = 1$.

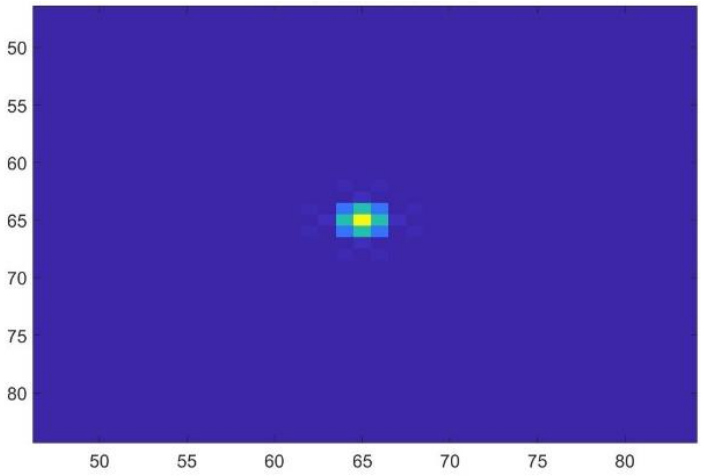

Figure 9: Non-turbulent PSF generated from a plane wave clearly shows perfect symmetry across the detector plane.

Comparatively, a turbulent PSF is shown in Figure 9. It is the result of aberrations in the respective wave front caused from atmospheric turbulence. In other words, its Zernike coefficients ≠ 0.

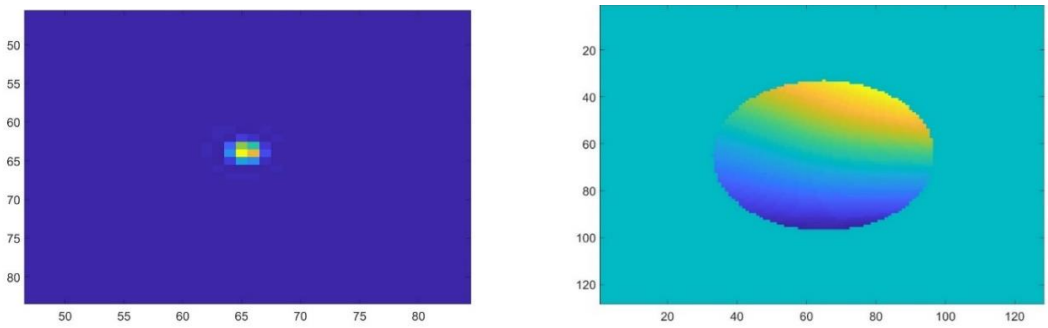

Figure 10: Turbulent PSF on the detector plane generated from a turbulent wavefront passing through simulated optical aperture.

3.1.3) Testing Motivation/Objectives

Understanding the primary focus for comparison of these phase unwrapping and phase retrieval methods is to understand how well they perform when implemented into an AO system. AO systems rely on making small adjustments to their components within milliseconds to measure and adapt to atmospheric turbulence. That is why this simulation will look to evaluate these methods based off of their speed, as well as their accuracy. This is in order to realistically evaluate the algorithms as if they were employed in a true WFS, where the atmosphere is changing on a millisecond timescale [5]. Concerning the accuracy of these algorithms, the sum squared error of the estimated phase screens with the true phase screen will be calculated once the resulting time restraint given by the AO system is expired, or when the algorithm has converged to an estimate.

Several of the phase retrieval methods use Zernike coefficients to generate their estimated wave fronts, which can then be used as another accuracy metric. As explained in Section 2.1.2 an existing wavefront can use

the inverse tactic and use the Zernike decomposition technique using Equation (2.5) to produce a set of coefficients based on a measured phase screen. Simply put, the difference between the sets of true Zernike coefficients and estimated coefficients become data that can also be compared for accuracy.

For the purpose of this simulation, the effectiveness of the two phase unwrappers will be assessed first. This will serve as a good segway and support piece to the phase retrieval evaluations to follow.

3.2) Phase Unwrapping Simulation

As stated prior, phase unwrapping methods are very important to phase retrieval methods and AO systems in general. Optical components and even phase retrieval methods like Gerchberg-Saxton can leave a system stuck with trying to unwrap a phase screen. Therefore, it is worth exploring and comparing the effectiveness of the LSU versus the GBU.

In order to simulate how well the LSU and GBU would theoretically work in an AO system, they will be tested to see how accurately and timely they can unwrap and converge to a true phase screen at different $D/r0$ values and different operating bandwidths.

3.2.1) Testing Procedure – Phase Unwrapping Methods

For the process of evaluating the phase unwrappers, phase screens with atmospheric noise are generated via Equations (3.3) through (3.6) using

$D/r0$ values between 0.7 and 2. This generates a true set of Zernike coefficients, $\vec{\hat{Z}}$, and a resulting true phase screen, $\hat{\theta}(x, y)$. In order to ensure most of the wavefronts that are being passed to the algorithms are wrapped wavefronts, a random piston value is added to the phase screen. The piston value, η, will be uniformly distributed between -π and π. Next, the phase angle of the true wavefront's field is calculated in order to produce a wrapped phase, $\tilde{\theta}(x, y)$.

$$\tilde{\theta}(x, y) = \angle e^{-j(\hat{\theta}(x,y)+\eta)} \tag{3.9}$$

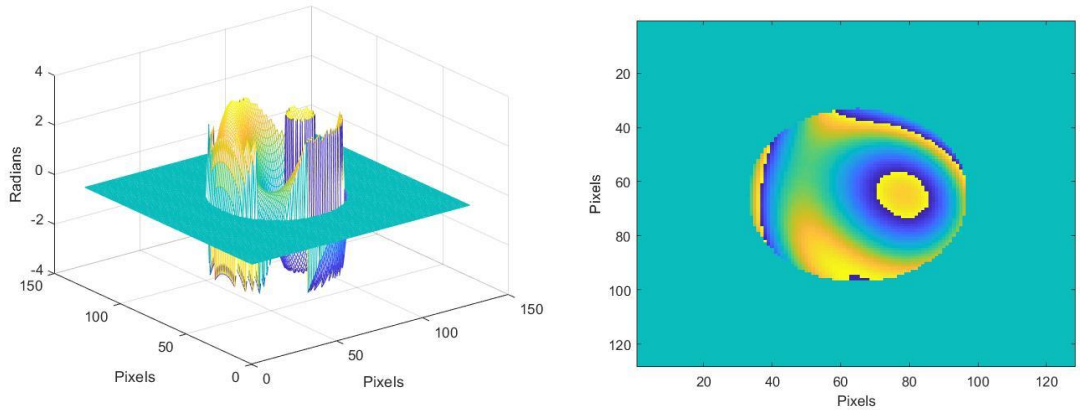

Figure 11: Example of a wrapped phase shows the discontinuity when phase values exceed π/- π radians.

This wrapped phase is one of two common inputs needed to compare the LSU and GBU. The other common input is the error threshold, ε. Between each iteration of the trial, the unwrappers will check if the absolute difference between the current iteration, i_n, and previous iteration's estimated unwrapped phase screen has changed less than ε. The arbitrary

error threshold value given to this input for the sake of the simulation is $1x10^{-8}$.

$$\varepsilon = 1\times10^{-8} = \sum_{y}\sum_{x}\left|\theta_{i_n}(x,y) - \theta_{i_{n-1}}(x,y)\right| \tag{3.10}$$

If the absolute difference between two consecutive iterations of each phase unwrapping method is less than ε, then the respective phase unwrapper will be considered 'converged.' This concludes that the algorithm will not need to conduct any more iterations of the respective algorithm, and that $\theta_{i_n}(x,y)$ is the algorithm's estimate of the true phase. The less amount of iterations a method takes to converge, the quicker and more often it will be able to update an AO system.

Another input needed for the simulation is the average iteration time for each algorithm. The average iteration time was averaged from 150 sample trials, with each trial having varying degrees of turbulent phase screens as inputs. Varying the degree of turbulence was determined by changing the $D/r0$ ratio values from 0.1 to 2. These time values become a feasibility baseline for each method when attempting to resolve the true phase screen in a time sensitive application. Their average iteration times, t_{avg}, are shown in Table1.

Phase Unwrapping Method	Iteration Time (sec/iteration), t_{avg}
Least Squares Unwrapper	0.00233
Gradient Based Unwrapper	0.00231

Table 1: Average iteration time for phase unwrappers.

Using these time values, one can calculate on average how many iterations can be accomplished in a trial. Given an AO system's operating bandwidth, bw, the maximum amount of iterations a method can manage in a trial of the simulation, $i_{\max}$, is simply:

$$i_{\max} = \frac{1}{bw \cdot t_{avg}} \tag{3.11}$$

These bandwidths will reflect certain operating speeds that AO system's physical components can operate at. In order to capture enough data to be statistically sound, the operating bandwidths will be increased from 1Hz to 300Hz, evaluating a set of 300 different wrapped phases at each observed bandwidth value. The $D/r0$ value will be varied to particular values of interest.

In each trial, a random, yet true, phase screen is built from its respective Zernike coefficients. Each phase unwrapping method will attempt to resolve the true phase screen with only their respective $i_{\max}$ values. Once the unwrappers converge or hit their iteration limit, each method will have produced a guess-phase screen, $\theta_{\text{method}}(x, y)$, that attempts to depict the true phase screen value, $\hat{\theta}(x, y)$. A set of estimated Zernike coefficient values,

$\vec{Z}_{\text{method}}$, can then be decomposed from the estimated phase screen. See Equation (2.5).

This guess-phase screen is the main output of the LSU and GBU algorithms, as they have attempted to reconstruct the complex waveform that was incident to the optical system's aperture given a measured PSF.

The following metrics aim to evaluate and compare the Least Squares Unwrapper against the Gradient Based Unwrapper's accuracy and their feasibility for use in an AO system.

1. The sum of the absolute differences between true and estimated Zernike coefficients.

$$zern\_err_{method} = \sum_{n} \left| \vec{Z}_n - \vec{\hat{Z}}_n \right|$$

2. Evaluate the algorithms at different bandwidths and different $D/r0$ values.

Metric 1 has one stipulation: During the decomposition from the phase screen into Zernike coefficients, both the GBU and LSU will occasionally attribute some of the aberrations to tilt (coefficients 2 and 3) when there should be no value for the tilt coefficients. This is due to the fact that our true phase screens are generated without tilt aberrations, but the phase unwrappers are not disallowed to calculate tilt as part contributor to the turbulence.

In order to account for instances where tilt is estimated to be a major aberration, a simple check is implemented to see if the sum of the magnitudes of z_2 and z_3 exceed 0.1. If this is the case, the algorithm is assuming the aberrations are largely caused by tilt and it is then considered "broken" and the iteration will not count. In real world scenarios, this could just be considered a skipped iteration in the control loop. The value of 0.1 was chosen to limit the number of breaks to below 30% in all instances of $D/r0 < 2$. Also, the number of "breaks" the GBU encounters has a linear relationship with the $D/r0$ value. It varies from 15.4% of the time at $D/r0 = 1$, up to 27.3% of the time at $D/r0 = 2$. See Table 2.

D/r0	Difference at imax = 3	GBU % Break	LSU % Break
0.7	0.00809	0.114396456	0.011074197
1	0.0032	0.154606866	0.044950166
1.1	0.00049	0.166987818	0.058361019
1.2	0.000045	0.178117386	0.073820598
1.5	0.00418	0.214119601	0.109590255
2	0.01089	0.273543743	0.16572536

Table 2: Rate at which generated wavefronts exceed tilt constraint for GBU.

3.2.2) Phase Unwrapping Results

Given their respective $i_{\max}$ values, the GBU and LSU method's accuracies were evaluated at varying bandwidths. Knowing that the unwrapper's performance changes based on the $D/r0$ value, the simulation was conducted at varying values between $D/r0 = 0.7$, and $D/r0 = 2$.

Observing the average absolute difference in Zernike's at the different bandwidths shows the pros and cons of both the LSU and GBU. Across all

simulations with the differing $D/r0$ values, it is easy to see that the LSU's average absolute difference in Zernike coefficients increases in a stepwise fashion. This is due to the decreasing amount of iterations the LSU is able to perform due to the bandwidth restrictions. Although more difficult to see due to the higher variance in the GBU's results, the average absolute differences for the GBU follow a stepwise pattern as well. The average differences of the unwrappers given an iteration count are shown on the graph to assist in showing these stepwise patterns.

Based on the findings, the average Zernike difference favors the LSU for all cases under 107 Hz. This corresponds to cases where the unwrapping methods are allowed to use 4 or more iterations. Upon reaching a bandwidth where only 3 iterations are executed, the results on which unwrapper has the lowest absolute Zernike difference varies based off of the $D/r0$ value. As long as $D/r0$ is roughly greater than 1.1, the GBU's Zernike decomposition outperforms the LSU. The results completely transition in favor of the GBU, independent of $D/r0$ value, when $i_{\max}$ is equal to 2 or less, or when an AO system's operating bandwidth is greater than 143 hertz.

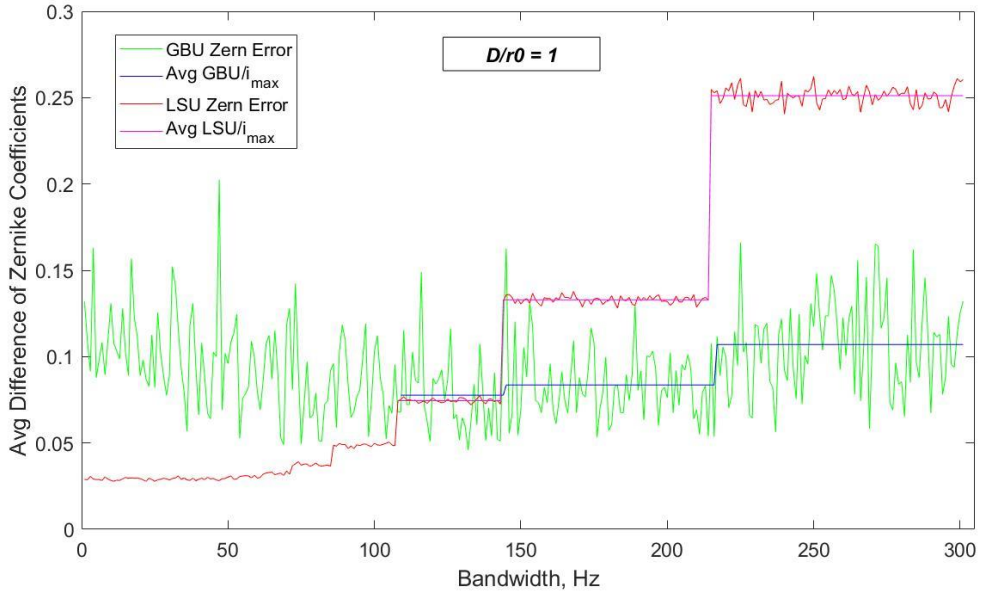

Figure 12: GBU and LSU performance with turbulence of D/r0 = 1.

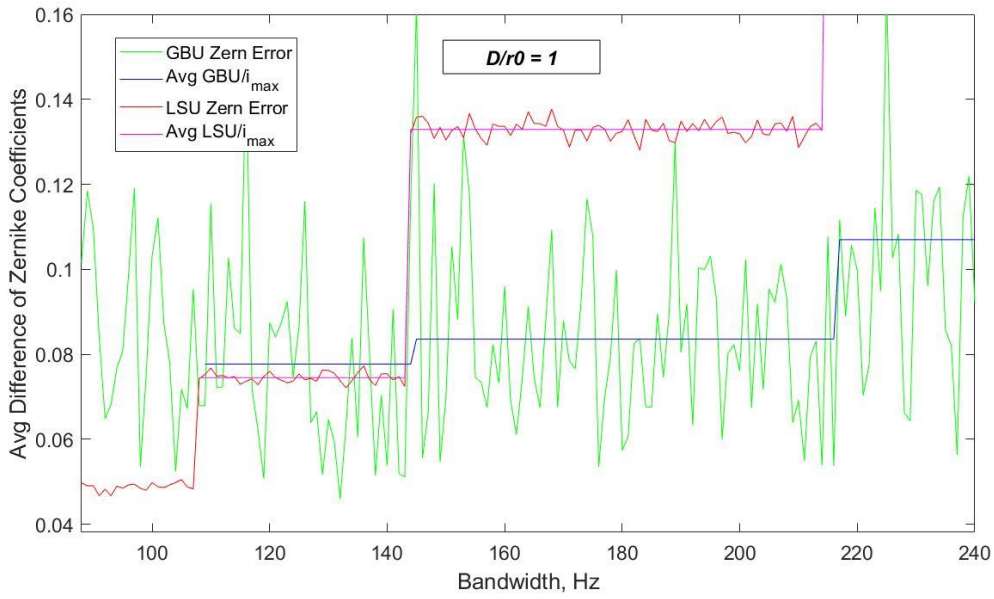

Figure 13: Close up of the GBU and LSU performance with turbulence of D/r0 = 1. The difference of the average values between 108 Hz and 143 Hz is approximately = 0.0032, in favor of the LSU.

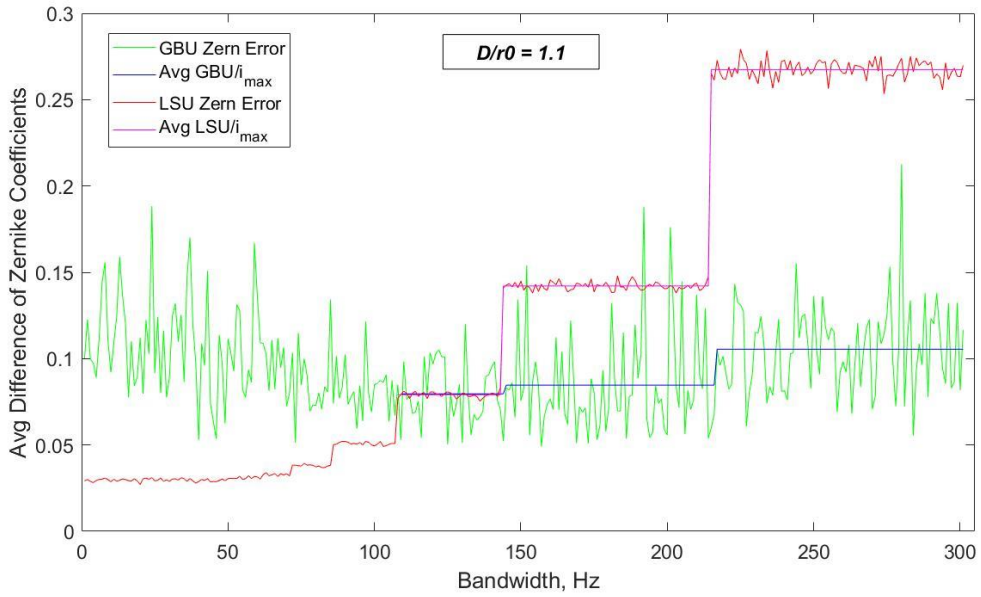

Figure 14: GBU and LSU performance with turbulence of D/r0 = 1.1.

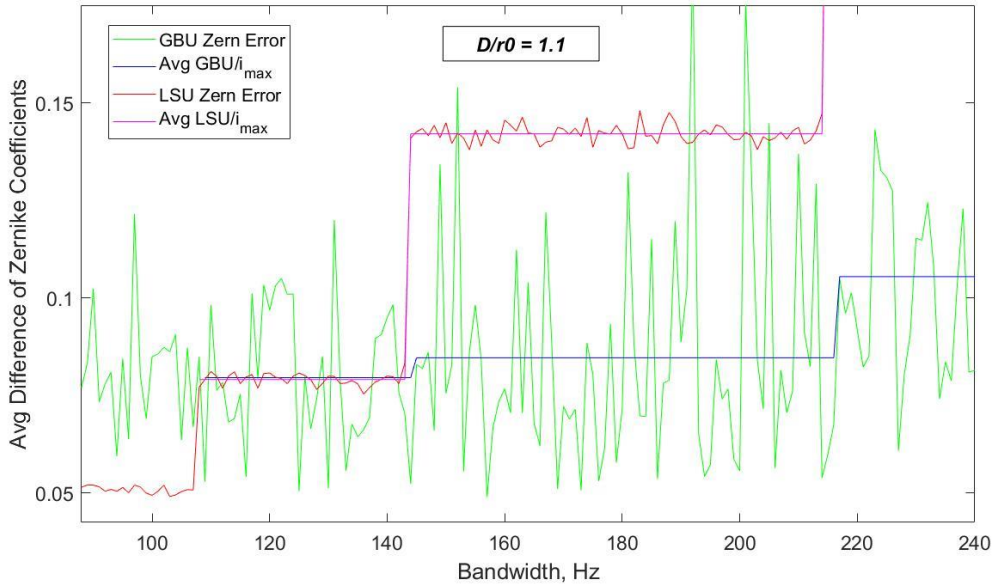

Figure 15: Close up of the GBU and LSU performance with turbulence of D/r0 = 1.1. The difference of the average values between 108 Hz and 143 Hz is approximately = 0.00049, in favor of the LSU.

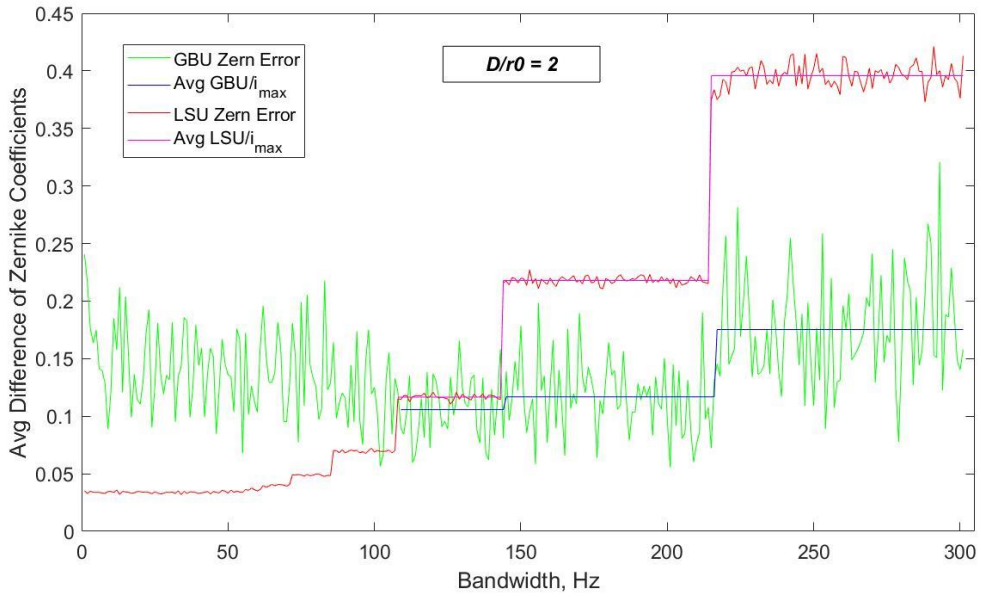

Figure 16: GBU and LSU performance with turbulence of D/r0 = 2.

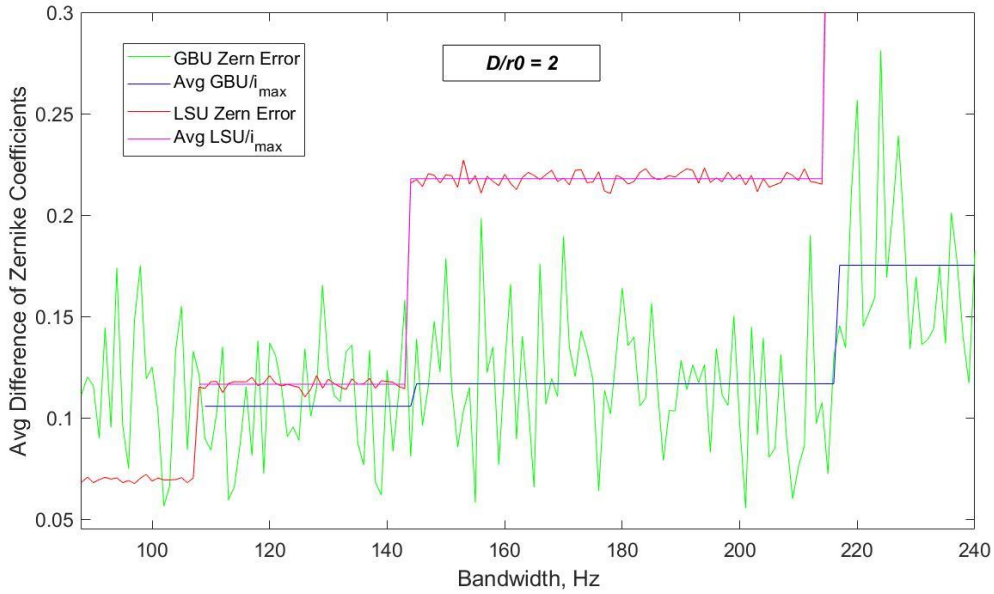

Figure 17: Close up of the GBU and LSU performance with turbulence of D/r0 = 2. The difference of the average values between 108 Hz and 143 Hz is approximately = 0.01089, in favor of the GBU.

In conclusion, the GBU phase unwrapping method performs better than the LSU when an operating bandwidth of 144 Hz or greater is required. And it could be said that the GBU would be the preferred method at operating bandwidths between 108-143 Hz even though it performs inferiorly to the LSU when $D/r0 < 1.1$. Due to the fact that the $D/r0$ ratio is close to 1 means that the optical system is better physically equipped to handle the amounts of atmospheric turbulence incident to the aperture than when $D/r0$ is larger. With the difference in the method's average values being roughly 0.0032 in favor of the LSU at $D/r0 = 1$, the argument could be made that the GBU is the better performing algorithm at all instances where an operating bandwidth of 108 Hz or greater is required.

3.3) Phase Retrieval Simulations

The next simulation will include a comparison of four phase retrieval methods. Attempting to recover and account for an atmospherically turbulent wavefront, given only the measurement of its PSF, is the cornerstone to AO systems. The more accurately and efficiently these wavefronts can be resolved, the more resolute an image can be formed in the detector plane of an optical system. Now that the differences between the two phase unwrappers have been explored, we can use them with some phase retrieval methods.

Since the Gerchberg-Saxton phase retrieval method produces a wrapped phase as an output, the simulation will run two instances of the method, one in conjunction with the GBU and one with the LSU.

In order to simulate how well the Gerchburg-Saxton with the Least Squares Unwrapper (GS-LSU), the Gerchberg-Saxton with the Gradient Based Unwrapper (GS-GBU), the Intensity Based Least Squares (IBLS), and the Electric-Field Correlation (EFC) methods would theoretically work in an AO system, they will be tested to see how accurately and timely they can converge to an unknown phase screen at different operating bandwidths given different $D/r0$ values.

3.3.1) Testing Procedure – Phase Retrieval Methods

To begin the simulation, 150 independent sets of Zernike coefficients are generated in order to produce 150 phase screens and consequently, 150 PSFs, at each varying bandwidth. These values become the simulation's truth data. The simulation calls for an iterative based approach where each PSF is assessed independently. As in the phase unwrapping simulation, the $D/r0$ values will be fixed when assessing the bandwidth capabilities but will occasionally be altered per simulation to explore areas of interest. The IBLS, EFC, GS-LSU and GS-GBU will be cross-examined using this Monte Carlo approach in order to measure results relating to the speed and accuracy of each method.

To begin each evaluation of the individual PSFs, the phase retrieval methods will be given the known aperture characteristics, $A(x, y)$, and true PSF, $\hat{I}_d(x', y')$ as common inputs. Each phase retrieval algorithm also requires a guess-phase as an input. For all simulations in this paper, the guess-phase for the IBLS and EFC methods will be a plane wave, meaning that all Zernike coefficients are initially equal to zero. Because using a plane wave as the first guess in the Gerchberg-Saxton algorithm seldomly results in meaningful data, a simple parabolic wavefront is generated as the initial guess phase. It is simply calculated using Zernike polynomial, $\phi_4(x, y)$, and a weighted coefficient estimated based off of application. In the case of this simulation, the coefficient, $z_4 = 0.2$.

No other inputs are needed to evaluate the GS-LSU and GS-GBU phase retrieval methods. However, the EFC and IBLS require a coefficient step value, Δ, which will be equal to 0.005 throughout this MATLAB simulation. All other specifics concerning the inputs given to the GS, IBLS and EFC methods are described in Chapter 2.

Once all of the proper inputs were fed to the phase retrieval algorithms, the average iteration time from 150 samples of each phase retrieval method was calculated to understand how quickly each method could operate. Using the same inspiration from the LSU and GBU assessment, evaluating how quickly each phase retrieval method operates is crucial to understanding its feasibility in AO systems. One thing of note is

that the two unwrapping method's times were calculated using the Gerchberg-Saxton method twice before passing it's wrapped phase onto the GBU and LSU. Two iterations of GS fostered the best results for the unwrappers due to the amount of noise added to the phase screen per iteration of GS. The average iteration time for the phase retrieval methods are shown in Table 3.

Phase Retrieval Method	**Iteration Time (sec), t_{avg}**
Intensity Based Least Squares	0.02084
Electric-Field Correlation	0.02004
Gerchberg-Saxton w/ GBU	0.00502
Gerchberg-Saxton w/ LSU	0.00504

Table 3: Average iteration time for phase retrieval methods.

Using these time values, we can calculate how many iterations can be accomplished in a simulation given a time restriction. In this simulation the bandwidth, *bw*, is increased with each simulation trial in order to evaluate how well each method can operate as the need for more iterations per second increases. Therefore, the maximum amount of iterations a method can generate in a trial of the simulation, $i_{\max}$, is simply calculated the same as Equation (3.11). Table 4 shows the maximum number of iterations per method.

Phase Retrieval Method	Maximum Iterations/second, i_{max}
Intensity Based Least Squares	47
Electric-Field Correlation	49
Gerchberg-Saxton w/ GBU	199
Gerchberg-Saxton w/ LSU	198

Table 4: Max iterations the phase retrieval methods can execute in a second.

One important thing to note is that after every iteration, the phase retrieval method's estimates of the phase screens are generated into PSFs and compared against the true PSF for error. This ensures that if any of the algorithms converge to an estimated PSF within an arbitrary error value of the true PSF, then that algorithm will stop, and the trial for that respective method will be considered complete. As with the phase unwrapping simulation, the arbitrary error threshold, ε, is set to $1x10^{-8}$. From here, the accuracy and speed within which each phase retrieval algorithm can recover an estimate of the true Zernike's, $\vec{\hat{Z}}$, are to be evaluated.

In order to capture enough data to be statistically sound, 150 trials will be conducted per given bandwidth value. In each trial, a random PSF is generated for the phase retrieval methods to try and resolve. Consequently, this means that each trial has separate truth data for a PSF, and it's Zernike coefficients. Each phase retrieval method will only be allowed to execute their respective max iteration values, i_{max}, and then will be stopped. At this point

in the simulation each method will have produced a set of estimated Zernike coefficient values, $\vec{Z}_{\text{method}}$, that attempt to depict the true phase screen value.

In order to thoroughly evaluate the capabilities of each method, several metrics are used to measure their accuracy and feasibility for use in an AO system.

1. The sum of the differences between true and estimated Zernike coefficients.

$$zern\_err_{method} = \sum_{n} \left| \vec{Z}_n - \vec{\hat{Z}}_n \right|$$

2. Evaluate the algorithms via metrics 1 and 2 at different bandwidths and different $D/r0$ values.

Using these metrics, this simulation will break down how well the aforementioned phase retrieval methods compare.

3.3.2) Phase Retrieval Results

The first thing that was noticed during the phase retrieval simulations was the poor performance of the GS-LSU. Due to the estimated output phase of the GS algorithm having several points of discontinuity and overall noisy characteristics compared to the wrapped phases tested in Section 3.2, the LSU struggled mightily to recover the true Zernike coefficients.

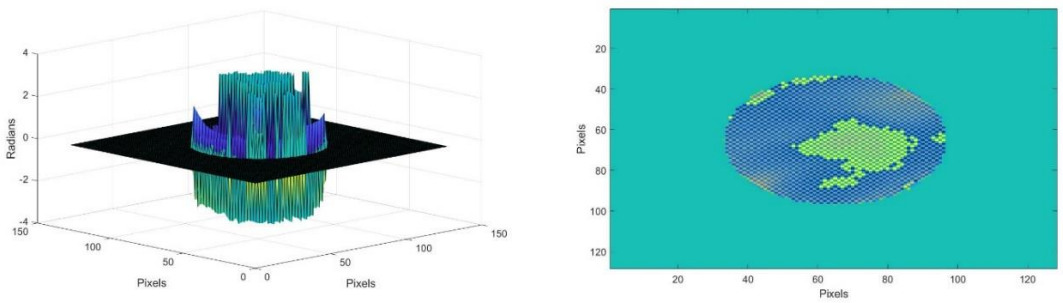

Figure 18: Noisy, wrapped phase outputted from the Gerchberg-Saxton

The sum of the absolute difference between true and GS-LSU estimated Zernike coefficients ranged between 15 and 40 – a full order of magnitude larger than the other three phase retrieval methods. This difference was consistent no matter the $D/r0$ value. See Figure 18 and Figure 19 below.

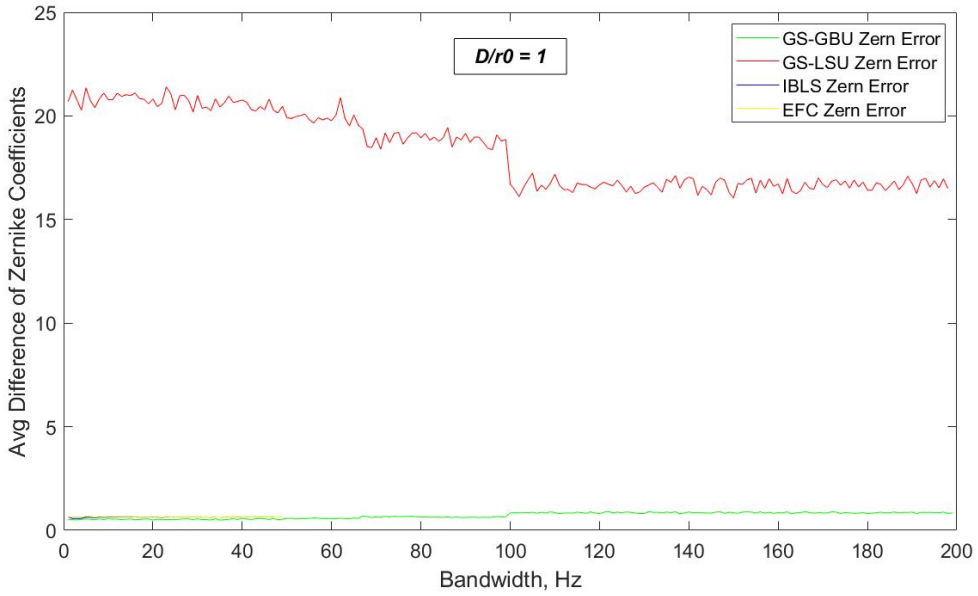

Figure 19: GS-LSU Zernike difference at D/r0 = 1 greatly exceeds difference of other phase retrieval methods.

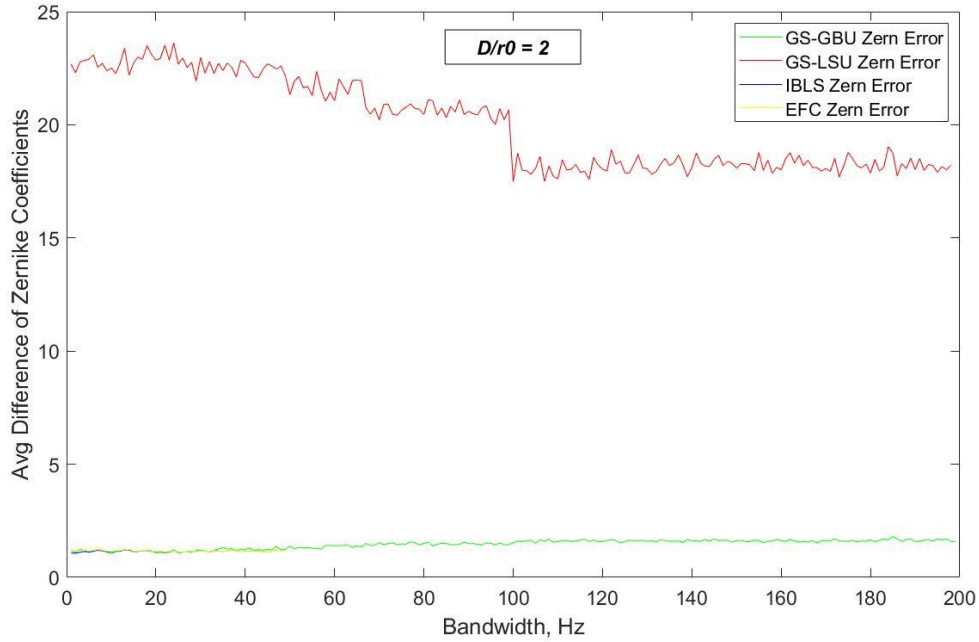

Figure 20: GS-LSU Zernike difference at D/r0 = 2 greatly exceeds difference of other phase retrieval methods.

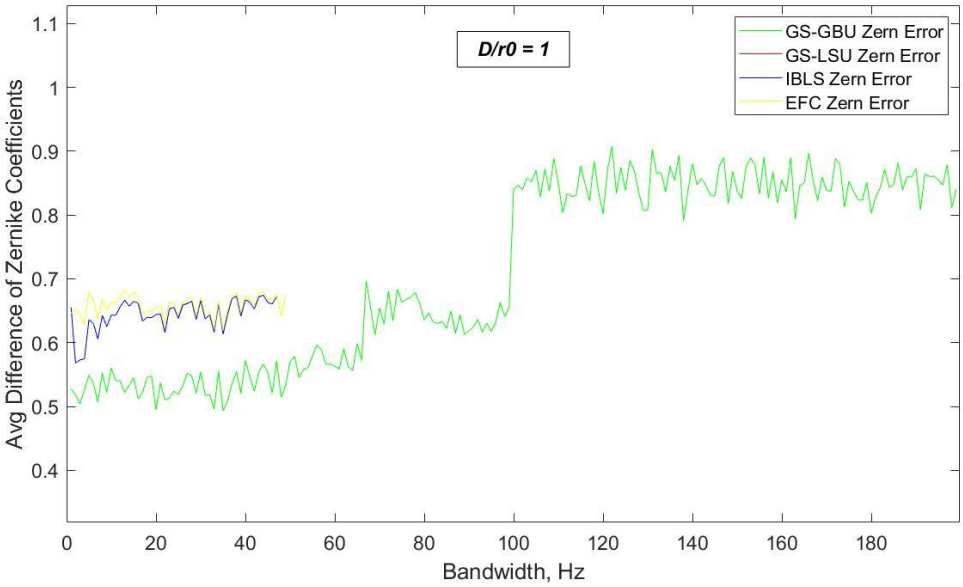

Figure 21: The GS-GBU outperforms the other phase retrieval methods at all bandwidths with D/r0 = 1.

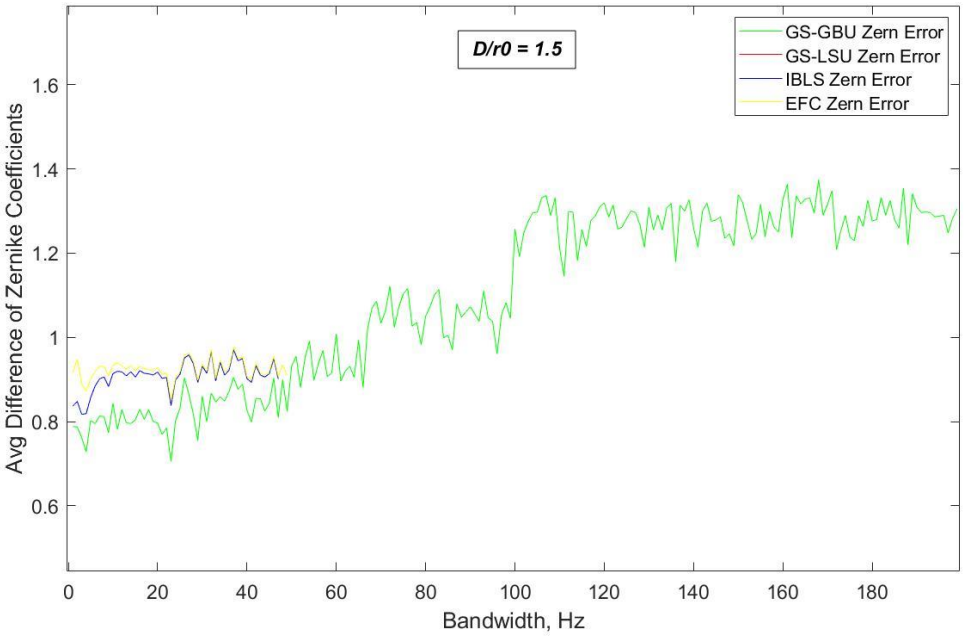

Figure 22: The GS-GBU outperforms the other phase retrieval methods at all bandwidths with D/r0 = 1.5.

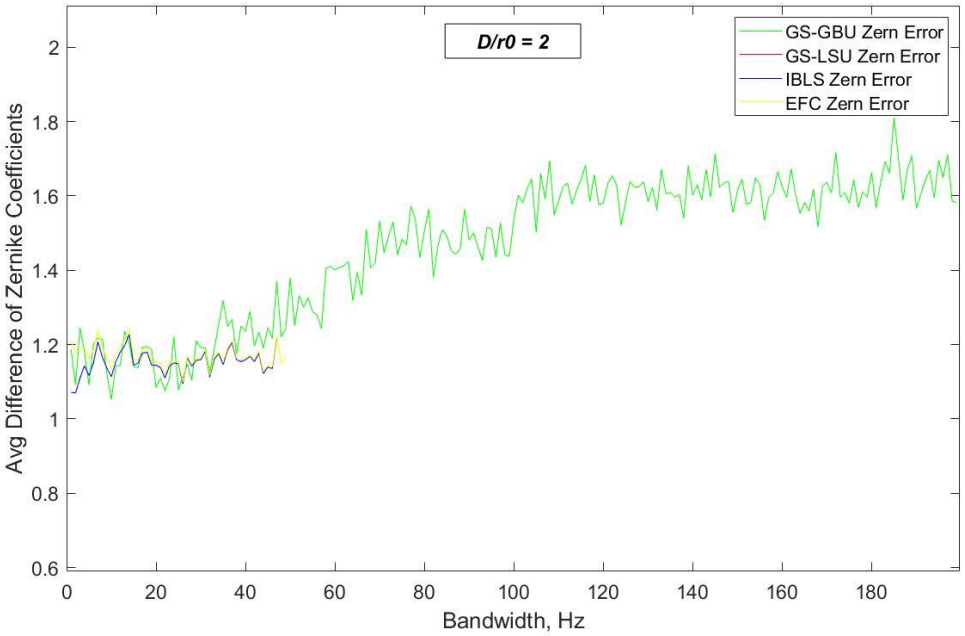

Figure 23: The GS-GBU and other phase retrieval methods have comparable differences from 1Hz – 47Hz at D/r0 = 2. However, the IBLS and EFC method's max bandwidth is much smaller than that of the GS-GBU.

The GBU algorithm worked much better given the noisy and discontinuous output phase from Gerchberg-Saxton, and therefore the GS-GBU method was more worthwhile to study versus the IBLS and EFC methods.

Based off of the simulation results, it is easy to see that the GS-GBU outperforms the IBLS and EFC no matter the bandwidth value and as long as $D/r0 < 2$. This bodes well for AO systems that would consider implementing the GS-GBU method, as it would have the ability to operate at higher bandwidths, and in most instances be able to more accurately account for the atmospheric turbulence incident to the optical system.

IV. Lab Simulation

It is constructive to observe the phase retrieval methods given real data. In this chapter we will explore the Gradient Based Unwrapper with Gerchberg-Saxton and the Least Squares Unwrapper with Gerchberg-Saxton with physical data created to simulate a ground-based telescope imaging through atmospheric turbulence.

4.1) Lab Setup

An LED with a 532nm wavelength was secured on an optical lab bench behind a pinhole, simulating a point source. The light was columnated and then propagated across the lab bench through 8 inches, or 20.3cm, of turbulent air into a circular aperture with a diameter of 5mm. Behind the aperture was a focusing lens that focused the light onto a camera's detector. The camera model used to capture the data was a ThorLabs 8050M-GE-8 camera with a 3296 x 2472 pixel detector. The pixel size was 5.5um x 5.5um.

The turbulent air was created using a variable heat source and blower that affected the lights path to the camera. The camera collected 200 images of the point source at a rate of 1 frame per second. The shutter speed, or integration time, of each frame was 20 milliseconds, with a gain of 120dB.

4.2) Evaluation Methodology

First, it was necessary to find the approximate seeing parameter value, *r0*, that was introduced to the experiment. Comparing the normalized

average of the collected intensity data with theoretical PSFs generated from long exposure optical transfer functions is one way we can approximate that environmental *r0* value.

Matching the width of the cross-section of the long exposure PSFs with the width of the cross-section of the average of the 200 data points, provided an *r0* value of approximately 3.3mm, giving the experiment an environmental *D/r0* value of 1.515. See Figure 23 below. Although the *D/r0* value is the same in all of the collected intensity measurements, just as in Chapter 3, the individual PSFs and frames collected of the point source are treated as statistically independent moments for the purpose of this thesis.

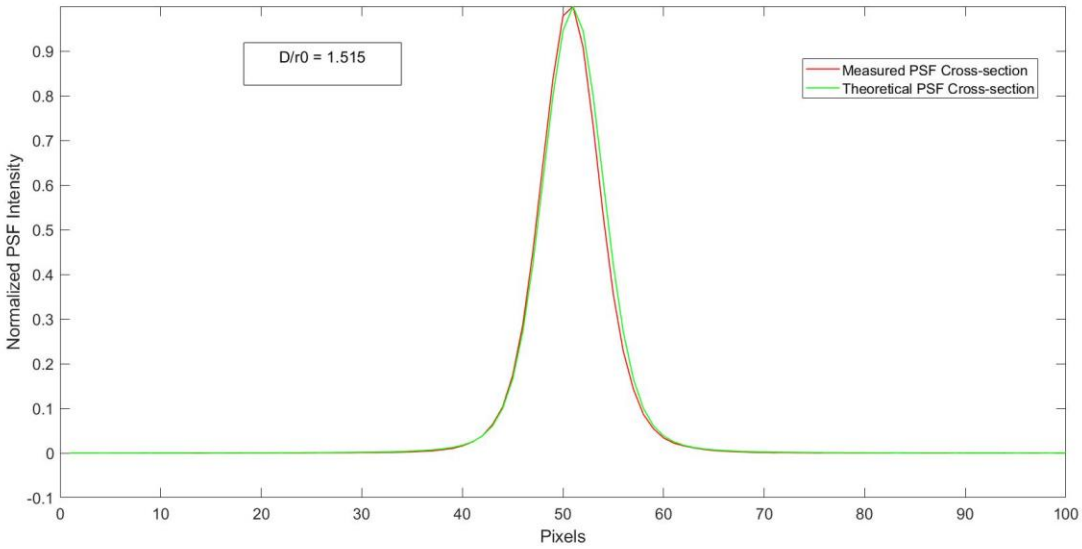

Figure 24: The cross-sections of the collected PSFs and the theoretical PSF given a D/r0 value of 1.515 match up nearly perfect.

After the seeing parameter was calculated, the images were cropped to 128x128 pixel matrices surrounding the PSF to allow for a more

computationally friendly process. The PSFs were further altered using the steps described below.

1. Filter out the background light.
   - Subtract each frame's median value from each respective pixel.
   - Zero-pad pixels surrounding the PSF.
2. Normalize the PSFs.
   - Zero-pad all remaining negative values in the frame.
   - Divide each PSF frame by the sum of its individual pixels.
3. Center the PSFs in the matrix to remove tilt.
   - This is normally accomplished in real data scenarios by using an intensity weighting algorithm.
4. Conduct GS-GBU and GS-LSU phase retrieval methods on collected/altered intensity measurements.

An example of a resulting altered frame ends up looking like Figure 24, on the following page.

Each frame will undergo a trial using the two phase retrieval methods and produce a set of Zernike coefficients for each respective method. The GS-GBU and GS-LSU will be limited to a bandwidth restriction of 108Hz or

quicker, implying that each method will use 3 iterations maximum for their respective phase unwrapper.

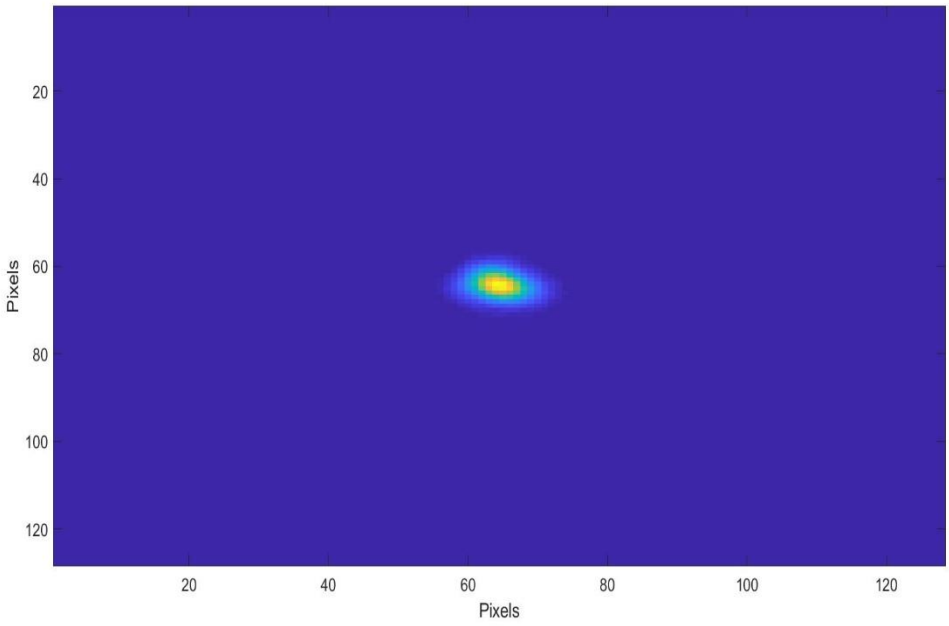

Figure 25: Example of an altered PSF for more simplistic computations.

Ensuring that Nyquist sampling criteria is met, the steps described in Section 2.2.3 and Section 2.2.4 are used with the lab PSFs and the known aperture to conduct 20 iterations of the Gerchberg-Saxton method before the estimated phase screen is handed over to the two unwrapping algorithms for comparison. Noise in the form of random piston error was implemented in order to ensure most of the resulting phase estimates passed on to the unwrappers by the GS algorithm were actually wrapped. The initial phase passed to the GS algorithm was a wavefront with 1/10 radians of defocus error (z_4).

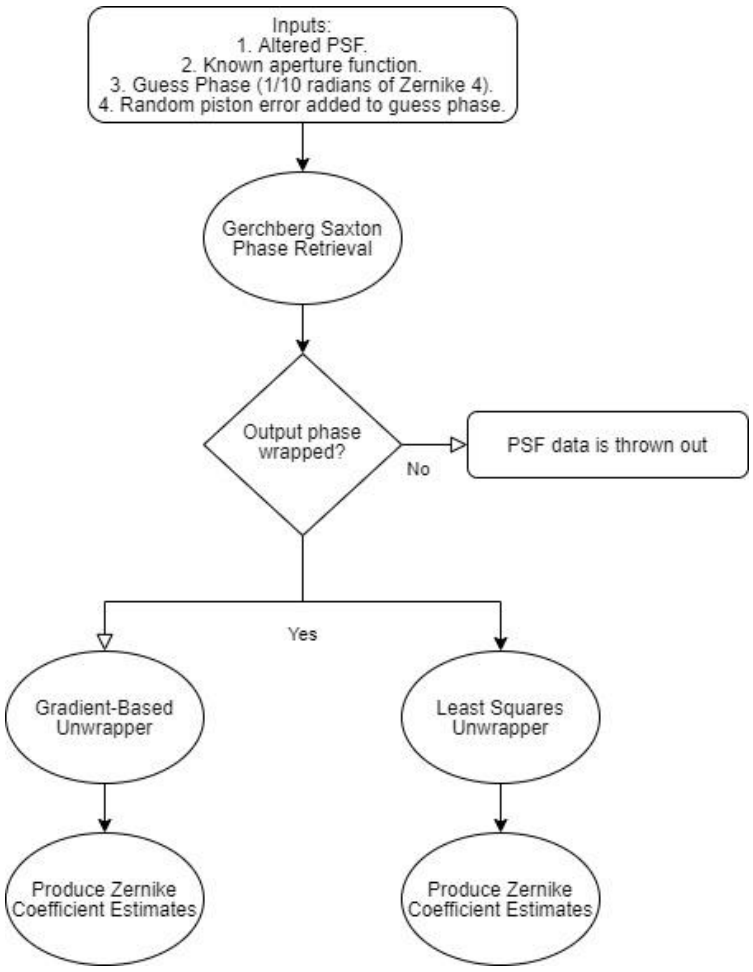

Figure 26: Flowchart explaining evaluation methodology.

It is useful for analytic purposes to know that Zernike coefficients are zero mean random variables that possess a given theoretical variance based on the D/r0 value. Calculating the mean and variances of the phase unwrapper's Zernike coefficients can give insight into how well the two phase retrieval methods are performing. The theoretical variances of Zernike coefficients 4-11, given $D/r0$, are shown in graph form below.

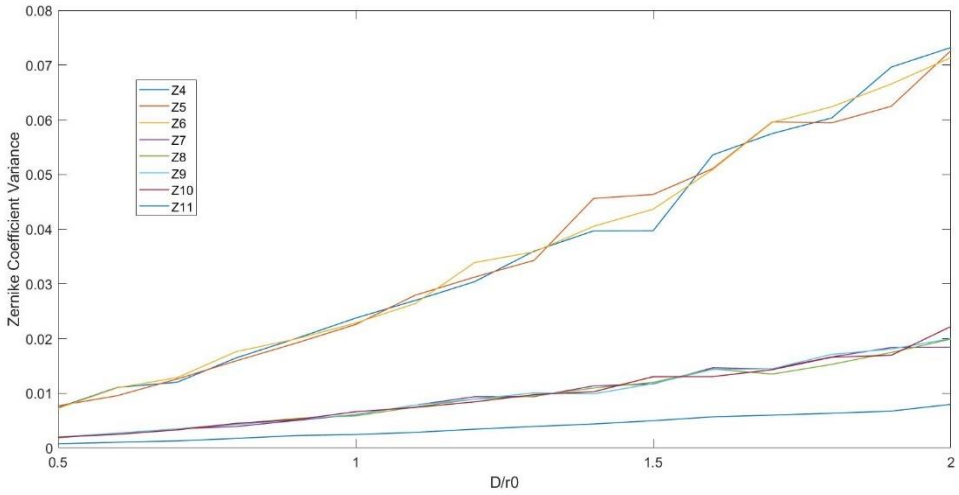

Figure 27: The groupings of Zernike polynomials given their variances as D/r0 increases.

4.3) Results from Lab Data

By excluding instances where the added piston error could not ensure a wrapped phase, the algorithm was given 113 out of the 200 frames to process. This infers that the other 87 frames did not have large enough aberrations to produce a wrapped phase after 20 iterations of Gerchberg-Saxton.

Next, using the data collected from the 113 trials, the means of the estimated Zernike coefficients were found and plotted to find out if the algorithms were producing realistic zero-mean Zernike coefficients.

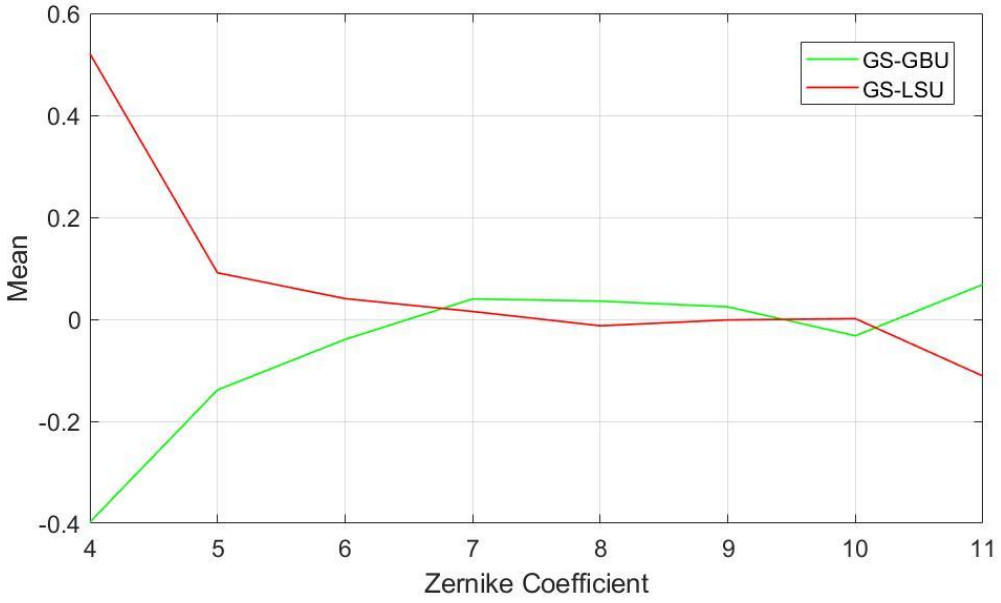

Figure 28: The means of the estimated Zernike coefficients derived from the GS-GBU and GS-LSU phase retrieval techniques.

First, it is easy to notice that z_4 (defocus aberration) and z_{11} (spherical aberration) have larger, non-zero mean, values. This is could be caused based off of the initial guess phase that is fed to the GS phase retrieval method. As stated in Section 4.2, the initial phase given to the GS method is a wavefront with 1/10 radians defocus error. Thus, having validated that the data collected is currently agreeable because the phase retrieval methods are estimating close to zero-mean Zernike values, another step to see how well the methods are performing is used by observing the variances in their calculated coefficients. The theoretical variances in Zernike coefficients for a $D/r0$ value of 1.515 are shown along with the calculated variances for the GS-GBU and GS-LSU methods.

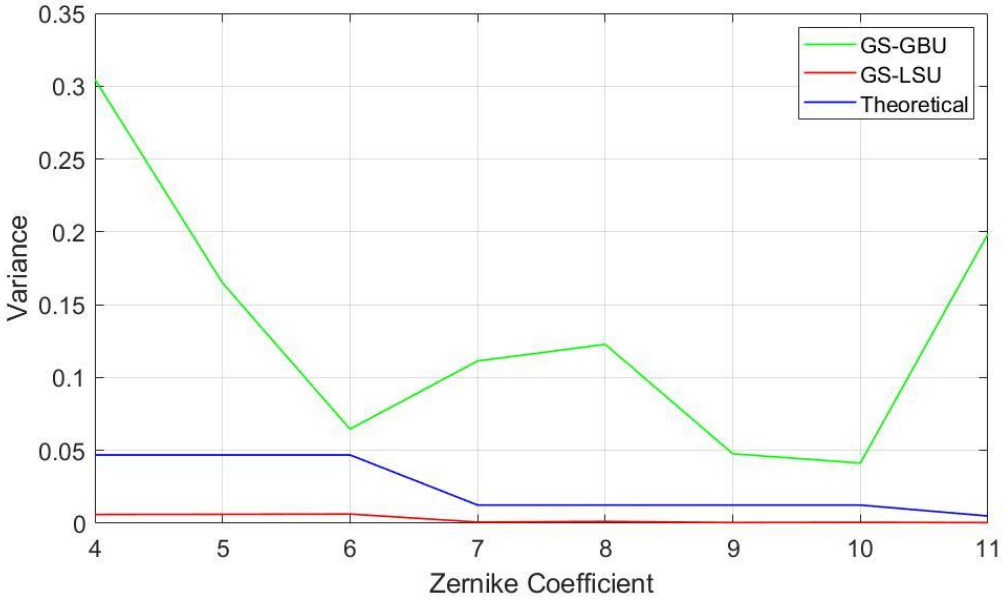

Figure 29: The GS-GBU variances are much more realistic to the theoretical by slightly exceeding them. The GS-LSU variances are much lower than should be expected.

Theoretical Coefficient Variances:

$z_4 - z_6 = 0.0469$, $z_7 - z_{10} = 0.0125$, $z_{11} = 0.005$

It is notable that the variances in GS-LSU's Zernike coefficients remain a full order of magnitude below the theoretical variances. This can be interpreted as the GS-LSU failing to properly conform to realistic wavefronts given a series of wrapped phases, either due to the discontinuity caused by the aperture or bandwidth restrictions.

The GS-GBU does not beat the theoretical variances in any instance - but it is close, which implies that its phase unwrapping algorithm is producing fair and sensible Zernike coefficients. This is evidence that when paired with the Gerchberg-Saxton phase retrieval method, the Gradient-Based Unwrapper is much more equipped to handle turbulent wavefronts at

higher bandwidths than the Least Squares Unwrapper, one of the industry standards.

4.4) Conclusion

Given the findings from the lab, it is satisfying to see the simulated data from Chapter 3 backed up by real lab data. It clearly shows that the GS-GBU is more capable of estimating phase values given a turbulent, wrapped phase. It produces much more sensible Zernike coefficients based on the comparison of their means and variances to the theoretical mean and variance values.

V. Conclusion

The evermore important matter of Space Domain Awareness motivates for more robust and efficient ground-based imaging methods. The Gradient Based Unwrapper used concurrently with the Gerchberg-Saxton Phase retrieval method gives those interested in imaging assets or hostile bodies in space a way forward to better resolve images saturated with atmospheric turbulence.

5.1) Thesis Conclusions

In this thesis the GBU demonstrates that it outperforms other phase unwrappers when put under conditions where higher bandwidths to perform phase retrieval efforts are required. The other phase retrieval methods prove to be either too cumbersome or too inaccurate to be viable options for phase retrieval when these bandwidth conditions are implemented.

The data gathered from the MATLAB simulations show that the GBU algorithm is always comparable or better than one of the industry's current standards when operating at bandwidths higher than 108Hz. This is an important data point for AO devices that work with very short exposure times, like daytime imaging. Lab results also show that when the atmosphere is extremely turbulent (based on a high $D/r0$ value) and there are high bandwidth requirements, the GBU can theoretically conform to a more accurate representation of what the true wavefront might look like based on

the calculations and comparison to the Zernike coefficient's theoretical variance. This is significant due to the fact that it was proved that the LSU does not have enough time to conform to a realistic wavefront based on the measured variances.

These findings provide wavefront sensors and other AO devices with an algorithm that can more accurately resolve turbulent images by quickly estimating the incoming phase, notably for daytime imaging.

5.2) Future Work

Moving forward with the exploration and implementation of the GBU includes trying to improve the algorithm by processing a set of temporally coherent intensity measurements and using their statistical dependence to more quickly estimate the fluctuation in the wavefront's shape between measurements. This infers that the r0 value would be calculated real-time by the AO system and passed to the GBU.

Another piece of future work with the GBU would be applying the algorithm in other lab scenarios and in real-time phase retrieval efforts that use AO devices. More data could be gathered using comparisons of the theoretical variance values in Zernike coefficients with differing $D/r0$ values. Collecting more real data would bolster the confidence in the GBU's theoretical and simulated results and prime it for implementation into AO systems.

Works Cited

1. D. of Defense, "UNITED STATES SPACE FORCE," 2019.

2. U. Congress, "National Aeronautics and Space Administration Authorization Act of 2005," pp. 2135–2321, 2005.

3. United Nations, *Technical report on space debris: Text of the report adopted by the Scientific and Technical Subcommittee of the United Nations Committee on the Peaceful Uses of Outer Space*. 1999.

4. J. L. Gustetic, V. Friedensen, J. L. Kessler, S. Jackson, and J. Parr, "NASA's Asteroid Grand Challenge: Strategy, Results, and Lessons Learned," *Space Policy*, vol. 44–45, pp. 1–13, 2018.

5. A. Tokovinin "Adaptive Optics Tutorial at CTIO" National Optical Astronomy Observatory, CTIO, May 28, 2001. [Online]. Available: http://www.ctio.noao.edu/~atokovin/tutorial/part3/wfs.html

6. J. W. Goodman, "Introduction to Fourier Optics, Second Edition," *Opt. Eng.*, vol. 35, no. 5, p. 1513, 1996.

7. I. B. Putnam and S. C. Cain, "Modeling a Temporally Evolving Atmosphere with Zernike Polynomials," *AMOS Tech. Conf.*, 2012.

8. "Zernike Polynomials" Wikipedia, 30 November 2019. [Online]. Available: https://en.wikipedia.org/wiki/Zernike_polynomials

9. J. C. Zingarelli and S. C. Cain, "Phase retrieval and Zernike decomposition using measured intensity data and the estimated electric field," *Appl. Opt.*, vol. 52, no. 31, p. 7435, 2013.

10. J. R. Fienup, "Phase retrieval algorithms: a comparison," *Appl. Opt.*, vol. 21, no. 15, p. 2758, 1982.

11. H. Xia *et al.*, "Phase calibration unwrapping algorithm for phase data corrupted by strong decorrelation speckle noise," *Opt. Express*, vol. 24, no. 25, p. 28713, 2016.

12. N. A. Roddier, "Atmospheric wavefront simulation using Zernike polynomials," *Opt. Eng.*, vol. 29, no. 10, p. 1174, 1990.

13. R. J. Noll, "Zernike polynomials and atmospheric turbulence*," vol. 06856, no. October 1975, pp. 207–211, 1976.

REPORT DOCUMENTATION PAGE

Form Approved
OMB No. 0704-0188

PLEASE DO NOT RETURN YOUR FORM TO THE ABOVE ADDRESS.

1. REPORT DATE *(DD-MM-YYYY)*	2. REPORT TYPE	3. DATES COVERED *(From - To)*
26 March 2020	Master's Thesis	Sept 2018 - March 2020

4. TITLE AND SUBTITLE

GLOBAL GRADIENT-BASED PHASE UNWRAPPING ALGORITHM FOR INCREASED PERFORMANCE IN WAVEFRONT SENSING

5a. CONTRACT NUMBER

5b. GRANT NUMBER

5c. PROGRAM ELEMENT NUMBER

6. AUTHOR(S)

Bartelt, Bryan R., Capt

5d. PROJECT NUMBER

5e. TASK NUMBER

5f. WORK UNIT NUMBER

7. PERFORMING ORGANIZATION NAME(S) AND ADDRESS(ES)

Air Force Institute of Technology
Graduate School of Engineering and Management (AFIT/EN)
2950 Hobson Way
Wright-Patterson AFB OH 45433-7765

8. PERFORMING ORGANIZATION REPORT NUMBER

AFIT-ENG-MS-20-M-006

9. SPONSORING/MONITORING AGENCY NAME(S) AND ADDRESS(ES)

Captain Joseph Tompkins
EO Target Detection & Surveillance Branch
2241 Avionics Circle
Sensors Directorate, AFRL
WPAFB, OH 45433-7765

10. SPONSOR/MONITOR'S ACRONYM(S)

AFRL/RYMT

11. SPONSOR/MONITOR'S REPORT NUMBER(S)

12. DISTRIBUTION/AVAILABILITY STATEMENT

Distribution Statement A. Approved for Public Release; Distribution Unlimited

13. SUPPLEMENTARY NOTES

14. ABSTRACT

As the reliance on satellite data for military and commercial use increases, more effort must be exerted to protect our space-based assets. In order to help increase our space domain awareness (SDA), new approaches to ground-based space surveillance via wavefront sensing must be adopted. Improving phase-unwrapping algorithms in order to assist in phase retrieval methods is one way of increasing the performance in current adaptive optics (AO) systems.

This thesis proposes a new phase-unwrapping algorithm that uses a global, gradient-based technique to more rapidly identify and correct for areas of phase wrapping during particular phase retrieval methods. This is beneficial in regard to the speed and accuracy within which a wrapped phase estimate is unwrapped using a new algorithm and doing so without having to change current AO systems or physical setups.

15. SUBJECT TERMS

Phase Unwrapping, Wavefront Sensors, Adaptive Optics

16. SECURITY CLASSIFICATION OF:			17. LIMITATION OF ABSTRACT	18. NUMBER OF PAGES	19a. NAME OF RESPONSIBLE PERSON
a. REPORT	b. ABSTRACT	c. THIS PAGE			Stephen Cain, Associate Professor
U	U	U	UU	72	19b. TELEPHONE NUMBER *(Include area code)* (937) 255-3636 ext. 4716 Stephen.Cain@afit.edu